HHS Public Access

Author manuscript

Med Phys. Author manuscript; available in PMC 2022 December 21.

Published in final edited form as:

Med Phys. 2022 April ; 49(4): 2794–2819. doi:10.1002/mp.15130.

Multi-parametric MRI (mpMRI) for treatment response assessment of radiation therapy

Chunhao Wang[1], **Kyle R. Padgett**[2,3], **Min-Ying Su**[4,5], **Eric A. Mellon**[2], **Danilo Maziero**[2], **Zheng Chang**[1]

[1]Department of Radiation Oncology, Duke University, Durham, North Carolina, USA

[2]Department of Radiation Oncology, University of Miami, Miami, Florida, USA

[3]Department of Radiology, University of Miami, Miami, Florida, USA

[4]Department of Radiological Sciences, University of California, Irvine, California, USA

[5]Department of Medical Imaging and Radiological Sciences, Kaohsiung Medical University, Kaohsiung, Taiwan

Abstract

Magnetic resonance imaging (MRI) plays an important role in the modern radiation therapy (RT) workflow. In comparison with computed tomography (CT) imaging, which is the dominant imaging modality in RT, MRI possesses excellent soft-tissue contrast for radiographic evaluation. Based on quantitative models, MRI can be used to assess tissue functional and physiological information. With the developments of scanner design, acquisition strategy, advanced data analysis, and modeling, multiparametric MRI (mpMRI), a combination of morphologic and functional imaging modalities, has been increasingly adopted for disease detection, localization, and characterization. Integration of mpMRI techniques into RT enriches the opportunities to individualize RT. In particular, RT response assessment using mpMRI allows for accurate characterization of both tissue anatomical and biochemical changes to support decision-making in monotherapy of radiation treatment and/or systematic cancer management. In recent years, accumulating evidence have, indeed, demonstrated the potentials of mpMRI in RT response assessment regarding patient stratification, trial benchmarking, early treatment intervention, and outcome modeling. Clinical application of mpMRI for treatment response assessment in routine radiation oncology workflow, however, is more complex than implementing an additional imaging protocol; mpMRI requires additional focus on optimal study design, practice standardization, and unified statistical reporting strategy to realize its full potential in the context of RT. In this article, the mpMRI theories, including image mechanism, protocol design, and data analysis, will be reviewed with a focus on the radiation oncology field. Representative works will be discussed to demonstrate how mpMRI can be used for RT response assessment. Additionally, issues and limits of current works, as well as challenges and potential future research directions, will also be discussed.

Correspondence Chunhao Wang, Zheng Chang, Department of Radiation Oncology, Duke University Medical Center, Durham, North Carolina, 27710, USA. chunhao.wang@duke.edu (C.W.), zheng.chang@duke.edu (Z.C.).

CONFLICT OF INTEREST

The authors have no conflicts to disclose.

Keywords

multiparametric MRI; response assessment; RT

1 | INTRODUCTION

Radiation therapy (RT) has been treating cancer for more than a century and has been adopted globally as an effective cancer management tool. It has been estimated that 50% of patients with cancer should receive RT in order to properly manage their diseases.[1,2] In the past decades, advances in technologies have significantly enhanced the landscape of modern RT. More specifically, rapid development and utilization of medical imaging, computerized treatment planning, and treatment delivery have enabled RT to evolve to ever increasingly complex forms of treatment delivery from conventional two-dimensional (2D) RT to three-dimensional (3D) conformal RT (3D-CRT), intensity-modulated RT (IMRT), volumetric-modulated arc therapy (VMAT), image-guided radiotherapy (IGRT), and stereotactic body radiation therapy (SBRT).[3]

Although numerous novel techniques have been adopted in the modern state-of-the-art RT, the workflow of RT generally remains unchanged. As illustrated in Figure 1a, the clinical workflow of RT can be divided into three stages: (1) treatment simulation with imaging scans: patients who are selected for RT are scanned with or without immobilization by CT and/or MRI. The use of immobilization is to ensure consistency of patient positioning. (2) Treatment planning: the CT and/or MRI data acquired during the simulation are used for the delineation of target volumes and critical organs-at-risk (OARs). Treatment plans including 3D-CRT, IMRT or VMAT could be selected and aim to deliver the prescribed radiation doses to the targets while minimizing the radiation to the surrounding critical OARs. (3) image-guided treatment delivery: in the treatment room, patients are positioned in the same manner as during the simulation stage. With the in-room image guidance, the locations of the targets are verified and confirmed before treatment delivery. Once confirmed, the treatment plans are delivered as planned. However, the current workflow might lack one important component: treatment assessment. If treatment assessment could be incorporated into the workflow as shown in Figure 1b, this would not only provide valuable insights into the effectiveness of RT, but also could help optimize treatment strategies for patients, potentially enhancing therapeutic outcomes and paving the road to individualized RT.

Currently, CT is the main imaging RT treatment planning, especially in external beam radiation therapy (EBRT), for its tissue density (electron density and mass density) information for dose calculation. CT is also frequently used for RT response assessment in terms of tumor/nodal volumes or spatial dimensions evaluation.[4-6] As a nuclear medicine approach, Positron Emission Tomography (PET) has been used for direct metabolic activity monitoring in RT. While PET imaging lacks anatomical detail, it is paired with a CT to provide co-registration with underlying anatomy. MRI has become a viable candidate for RT treatment planning and response assessment. Since its onset, MRI has evolved from anatomic imaging to angiographic imaging to physiologic imaging, offering numerous clinical applications. As demonstrated in Figure 2, MRI is heavily utilized, in many

cases mandatory, in the treatment planning for stereotactic radiosurgery (SRS), which is an effective treatment for the management of brain metastases, acoustic neuroma, arteriovenous malformation (AVM), and other brain diseases.[7-9] In addition to standard anatomic imaging, MRI offers various quantitative functional imaging techniques including, but not limited to, diffusion-weighted imaging (DWI), diffusion tensor imaging (DTI), MR spectroscopy (MRS), and dynamic contrast-enhanced (DCE) imaging. DWI can be used to assess the changes in cellular density. MRS is used to assess biochemical changes non-invasively. DCE-MRI evaluates changes in the microvascular environment with fast imaging and injection of contrast agents. Recently, multi-parametric MRI (mpMRI) has been introduced, which includes multiple functional parameters derived by the above functional imaging techniques along with standard anatomic imaging.[10,11] Early data have suggested that mpMRI could be a promising and valuable tool for both diagnosis and treatment assessment.[10-12] In contrast to other functional imaging modalities such as positron emission tomography (PET) and single-photon emission computed tomography (SPECT), mpMRI has the appealing feature of providing both anatomical and functional information in a single imaging session, often with improved spatial resolution.[13] Furthermore, mpMRI has zero ionizing radiation risk. This attractive feature allows mpMRI to be an excellent candidate for longitudinal clinical studies, which generally require repeated acquisitions over a period of time.

RT response assessment with mpMRI requires multiple imaging sessions including before, during, and after the treatment to assess radiation-induced functional changes in tumor targets and/or OARs.[14] The captured early functional change by mpMRI could potentially be used to optimize the treatment strategy including altering the fractionation schedule, dose escalation, and refinement of tumor targeting. mpMRI might serve as an indispensable tool toward individualized RT.

2 | QUANTITATIVE IMAGING IN mpMRI

As previously discussed, mpMRI has been referred to as any form of MRI that involves multiple functional quantitative parameters in supplement to standard anatomical MRI imaging.[10,11] With inherent quantitative natures, mpMRI can capture information of underlying tissue characteristics in biochemical and physiological processes through various quantitative MRI (qMRI) methods, which includes, but are not limited to, diffusion-weighted imaging (DWI), diffusion tensor imaging (DTI), dynamic contrast-enhanced MRI (DCE-MRI), magnetic resonance spectroscopy (MRS), blood oxygen level-dependent (BOLD) MRI, and other emerging qMRI techniques.

2.1 | Diffusion-weighted MRI

Diffusion-weighted MRI is sensitive to the random Brownian motion of water molecules in tissue.[15] The degree of restriction to the random motion of water is correlated to the tissue cellularity and the cell membrane integrity[16]: in tissues with high cellular density with intact cell membranes, extracellular water molecule diffusion is more restricted than areas of low cellular density with the possibility of breached cell membrane.[17] DWI captures the amount of diffusion via MR phase-shift sensitivity in a pair of reversed gradient pulses.

The weighting of the applied gradients is represented by a *b*-value that combines amplitude, duration, and the interval between paired pulses.[18] DWI is typically performed using at least two scans with different *b*-values. While a larger *b*-value scan has lower signals from water molecules, the relative signal attenuation from a small *b*-value scan (typically 0) to a larger *b*-value scan (typically >500 s/mm^2) can characterize water diffusion heterogeneity in tissue. As such, the coefficient of mono-exponential attenuation in MR signals with two different *b*-values, apparent diffusion coefficient (ADC), has been adopted as a quantitative biomarker of water diffusion degree. To date, ADC has been reported in numerous studies of disease detection, treatment response assessment, and outcome prediction. Nevertheless, the relatively simple mono-exponential approach cannot separate extravascular-extracellular space (EES) water diffusion from microvascular perfusion. To address this issue, intravoxel incoherent motion imaging (IVIM) was proposed to utilize a biexponential model to model EES water diffusion and vascular perfusion flow separately.[19]

2.2 | Diffusion tensor imaging

Following the same physical principles in DWI, diffusion tensor imaging (DTI) intends to capture the direction information of anisotropic water molecule diffusion in tissues. Unlike the scalar presentation of ADC in DWI, DTI characterizes diffusion anisotropy by a symmetric tensor ***D*** that describes water molecular mobility along each direction and the correlations between each direction pair.[20] To determine ***D***, diffusion-weighted images with diffusion-sensitized gradients in several directions are needed. A classic 6-direction gradient encoding set has been widely adopted to determine the symmetric ***D***. Following the introduction of diffusion tensor formalism,[21] DTI data can be quantitatively interpreted by fractional anisotropy (FA), which is a fraction between 0 (isotropic diffusion) and 1 (restricted directional diffusion with elongated ellipsoid) as diffusion directional homogeneity descriptor derived from the eigenvalues of diffusion coefficients along three orthogonal directions.

The topic of water diffusion anisotropy in DTI is of particular interest in the central nervous system imaging of the brain and spinal cord. Intracranial FA map results demonstrate excellent brain tissue segmentation: In white matter, the typical high anisotropy (approaching unity) results suggest rapid water diffusivity along the fibers and slow diffusivity perpendicular to the fibers[22]; in CSF and gray matter, the typical low anisotropy results suggest isotropic water diffusion. By utilizing the rotational invariance of DTI, neuro fiber tracking that extracts 3D alignment of diffusivity in white matter becomes possible.[23] Current 3D fiber tractography can be used to study connectivity as well as the architecture of the healthy brain and to detect white matter damages for compromised sensory and neurocognitive functions.[24]

2.3 | Dynamic contrast-enhanced MRI

Dynamic contrast-enhanced MRI (DCE-MRI) studies the dynamics of injected contrast agent (CA) in tissue by a sequential imaging acquisition before, during, and after T1-shortening CA injection.[25] When CA enters soft tissue, the T1 value decreases to an extent determined by the CA concentration, which is reflected by elevated apparent imaging signal in T1w images. Thus, after repetitive T1w acquisitions in a tissue region-of-interest (ROI),

MR signal evolution as a function of time can be observed within each imaging voxel, and an ROI MR signal evolution curve can be generated using ROI-averaged MR signal at each imaging frame.

The semi-quantitative approach of the DCE-MRI study focuses on MR signal evolution curve analysis. Semantics of the MR signal evolution curve, such as peak enhancement and early drop, can be used for disease classification.[26] Simple numerical descriptors of the MR signal evolution curve, including initial Area Under the CA-time Curve (iAUC), enhancement ratio, early contrast uptake, and time lag between CA injection and MR signal enhancement, have been proposed as parameters for disease detection in DCE-MRI.[27]

In quantitative approaches of DCE-MRI analysis, CA concentration evolution in tissue can be estimated from T1 value change from pre-CA basline.[28] A few methods exist for rapid T1 value quantification using MR signal changes.[29,30] Pharmacokinetic (PK) models are used to fit CA concentration evolution curves in voxel-level or ROI implementation. The derived PK model parameters are associated with micro-vessel permeability, vessel perfusion rate, and cellular density with certain PK model assumptions. While adiabatic approximation of CA dynamics has been reported,[31] most common PK models assume CA transport between tissue compartments. A classic compartmental model in DCE-MRI is the Tofts model, which describes the bi-directional transendothelial movement of CA molecules between blood plasma and EES through capillary walls.[32] The CA extravasation rate K^{trans} has been reported as the most common DCE-MRI quantitative biomarkers. Additionally, EES volume fractions, blood plasma volume fractions, CA return rate, and intracellular water lifetime during CA extravasation are also analyzed by different Tofts-like two-compartment PK models.[28,33,34] Meanwhile, multi-compartment models can potentially describe CA dynamics more accurately[35]; however, complex model interpretation limits the applicability of this type of PK model. To solve compartmental PK models, CA dynamics in blood plasma after administration, also called Arterial Input Function (AIF), must be known. This knowledge can be achieved by imaging a major blood pool inside the imaging field-of-view during DCE-MRI scan.[36,37] When such measurement is not available, alternative approaches include the adoption of population-averaged AIF[38,39] and estimate AIF from a reference region as a semi-parametric approach.[40]

2.4 | Dynamic susceptibility contrast MRI

As another dynamic MRI procedure, dynamic susceptibility contrast (DSC) imaging utilizes the susceptibility induced signal loss on T2*-weighted sequences from CA in the dynamic imaging.[41] DSC-MRI exploits the regional susceptibility-induced signal loss caused by (super)paramagnetic CA on T2w images. Through rapid repeated T2*-weighted sequences (such as gradient echo-planar imaging), DSC acquires a series of images with signals representing intrinsic tissue T2* signal attenuated by susceptibility-induced signal loss, which is proportional to the amount of CA in the vascular structures.[42] T2-weighted approach of DSC implementation may be feasible with higher dosage of CA injection.[42,43] DSC-MRI is the method of choice for the measurement of cranial blood perfusion parameters with MRI, including cerebral blood flow (CBF) and cerebral blood volume (CBV), and mean transition time (MTT),[44] and these parameters have been reported to

monitor brain RT outcomes. Nevertheless, accurate quantification of cranial blood perfusion remains challenging after years of clinical application; inherent blood/tissue relaxivity difference may lead to scaling errors in CBF and CBV results.[45] As such, DCE-MRI has become an alternative solution for cranial blood perfusion quantification with negligible T2* shortening effect using short echo time.[46]

2.5 | Magnetic resonance spectroscopy

Following the spectroscopy concept in chemistry, magnetic resonance spectroscopy (MRS) aims to discover certain tiny metabolite molecules in intracellular and extracellular spaces.[47] The achieved spectra provide detailed information about metabolites, thus MRS can evaluate disease-induced or treatment-related metabolic variations on a molecular scale.[48] In MRS applications, smaller signals from the targeted metabolites are weak but of more clinical interest, and thus high magnetic field strengths are typically used to ensure adequate signal-to-noise ratio (SNR).[49] While several common nuclei in the human body are available for spectra acquisition, including ^{1}H, ^{13}C, ^{19}F, and ^{31}P, ^{1}H is often chosen for MRS since ^{1}H exists in a large number of metabolites and ^{1}H has a high concentration making it easier to detect than the other nuclei. In single voxel spectroscopy (SVS), a single voxel of tissue is chosen for spectrum derivation, and the voxel location is often determined by anatomical MRI guidance.[49,50] As another MRS approach, chemical shift imaging (also called MRSI) can acquire multiple voxels' spectrum simultaneously within a larger imaging volume (needs ^{1}H signal suppression[51,52]) to capture spatial heterogeneity.[53] In clinical studies, MRS application is relatively limited due to intensive MR specialties, long imaging acquisition time, high study cost, and the reported low sensitivity.[54] Nevertheless, due to the high sensitivity of metabolites variation, MRS in medicine has been focusing on the neural imaging of brain diseases, while its extracranial applications have also investigated.[55]

2.6 | Bold MRI

Hypoxia is an important cause of radio-resistance in RT of solid tumors. It occurs when oxygen delivery to tissue is inadequate due to disordered angiogenesis.[56] As an imaging-based in vivo measurement tool, blood oxygen level-dependent (BOLD) MRI utilizes the susceptibility sensitivity to paramagnetic deoxyhemoglobin monomer (Hb), which increases the MR signal transverse relaxation rate ($R2^* = 1/T2^*$) of water in the blood and surrounding tissue.[57] While R2* did not directly measure tissue oxygen concentration, it can infer oxygenation status via capturing the heterogeneous R2* distribution in reference to perfused blood pools. Thus, BOLD MRI can measure the oxygen level in tissues adjacent to blood vessels.[58] A similar MRI technique, tissue oxygenation level-dependent (TOLD) MRI, detects tissue hypoxia with longitudinal relaxation rate ($R1 = 1/T1$) change by heterogeneous Hb distribution.[59] Both BOLD MRI and TOLD MRI can be used to capture potential re-oxygenation following the irradiation of solid tumors.[60] Additionally, BOLD MRI results are of interest as surrogate biomarkers to identify solid tumors with potentially poor RT outcome.[61]

2.7 | Other emerging qMRI methods

Several emerging functional quantitative imaging techniques have become more accessible for oncology application. General MR relaxometry intends to isolate the contributions of

individual MR contrast mechanisms and provides metrics in absolute units, which can serve as noninvasive surrogates for pathology and histology.[62] Its recent development, MR fingerprinting (MRF),[63] acquires tissue-type-specific signal evolutions (i.e., fingerprints) acquired by pseudorandom variation of MR system setting during data acquisition. Acquisition from individual voxels is compared with a collection of simulated fingerprints in a library, and the best match for the voxel fingerprint is selected from the library through a pattern matching process.[64] Thus, the underlying tissue property (T1, T2, and proton density) and functional characteristics (such as brain perfusion[65,66]) can be quantitatively measured. Chemical exchange saturation transfer (CEST) MRI is a novel imaging technique with potentials to provide molecular information for diagnosing pathological tissues and monitor molecular responses to treatment.[67] CEST images certain compounds at concentrations that are too low to directly be detected in MRS at typical water imaging resolution[68]; a good clinical application is amide proton transfer (APT) imaging, which can present the pH-weighted map to monitor abnormal cerebral blood flow.[69] T1 rho (T1p) imaging is a novel imaging mechanism that uses a long duration low power radiofrequency (i.e., spin lock) applied to the magnetization in the transverse plane. This design effectively locks the magnetization vector without phase decay as in a rotating frame, and the decay of the locked magnetization depends on both T1 and T2 of the tissue.[70] Promising applications of T1 rho imaging have been demonstrated in preclinical studies of musculoskeletal imaging.[71,72] Hyperpolarized MRI greatly increases the detectability of certain metabolites using non-hydrogen nuclei. In cancer imaging, ^{13}C has been reported in hyperpolarized MRI for necrosis detection,[73] perfusion,[74] and lactate-based cell proliferation.[75] Although these emerging techniques remain at their early preclinical stages in RT response assessment, more studies are expected in the future with enriched functional information.

In addition to the quantitative MRI methods, an emerging field of radiomics becomes a leading example of quantitative imaging analysis. Radiomics aims to transform standard-of-care medical images into mineable data for computational biomarker extraction in high throughput implementations.[76] These biomarkers—so-xcalled radiomic features—can be used to non-invasively detect tissue underlying histopathology and therapeutic responsiveness. Radiomics can be applied to both anatomical MRI images as well as functional quantitative MRI images and the associated parametric results. A more thorough review of radiomics theory and application can be found in other dedicated literatures.[77,78]

3 | mpMRI IN RT TREATMENT RESPONSE ASSESSMENT

This section reviews the representative mpMRI applications in RT response assessment. While representative works at common mpMRI anatomical sites are discussed in detail, mpMRI applications at other RT sites are also summarized.

3.1 | Brain

Glioblastoma (GBM) accounts for almost half of all malignant tumors originating in the brain, and it is characterized by deep invasion at the time of diagnosis, high cellularity, frequent cell division, existence of necrosis, and increased vascularity.[79,80] Standard treatment for GBM includes surgical resection to remove as much tumor tissue

as possible without significant effects on quality of life followed by 6 weeks of RT with concurrent temozolomide chemotherapy and at least 6 months of additional temozolomide chemotherapy.[81] In the best prognosis of patients treated with modern therapies, median survival for GBM is about 21 months with few patients surviving the past 5 years.[82,83] Response assessment is challenging in GBM.[84] Attempts to classify response based on anatomic changes using standardized criteria are often based on Response Assessment in Neuro-Oncology (RANO) criteria[85] using T1 post-contrast enhancement, reflecting tumor hyper-vascularity. However, portions of the tumor can also be non-enhancing and visible only as T2/FLAIR hyper-intensity which is easily confused for benign edema or hidden on conventional MRI any intermixed with normal-appearing brain.[86] A common diagnostic dilemma begins with the first MRI after chemo-RT. Up to half of all GBMs exhibit increased contrast-enhanced volume in early follow-up imaging.[87,88] Similar growth has also recently been described during chemo-RT.[89] These short-term volume changes can represent true progression or pseudoprogression. True progression represents non-responding tumor that continues to grow on serial MRIs without intervention, while pseudoprogression reflects the response to treatment including neovascularization and tumor necrosis and stabilizes or spontaneously regresses without treatment modification usually within 6 to 9 months.[90-92] It is important to distinguish these possibilities since patients with true progression have a poor median survival on the order of 8 months after chemo-RT completion, while patients with pseudoprogression have a median survival on the order of 3 years after chemo-RT completion.[88] Another common diagnostic dilemma occurs later after chemo-RT. Recurrence of GBM can occur many months or years after treatment. However, radiation necrosis, a severe local tissue reaction to radiation with necrosis of normal brain tissue and neovascularization, can also occur many months or years after chemo-RT.[93,94] Figure 3 demonstrates an example of mpMRI analysis for the GBM RT assessment.

In pseudoprogression differentiation from poorly responding glioblastoma, ADC from DWI is known to correlate with tumor cell density before chemo-RT.[95,96] During chemo-RT, increases in ADC values are associated with longer survival compared to decreases in ADC.[97] Similarly, post-treatment elevated minimum and mean ADC results are significantly related to Overall Survival and Progression-Free Survival.[98,99] Similar to diffusion, higher values of relative CBV (rCBV) from DCE-MRI perfusion studies are noted for patients with tumor progression compared to patients with pseudoprogression.[100,101] Comparing pre- and post-treatment MRIs, survival is better for patients with decreased rCBV compared to patients with increased rCBV.[102] Additionally, patients with improved survival after chemo-RT were reported with larger increases of K^{trans} and small or no increase of CBF from DCE-MRI studies.[103] Tumor response to therapy can also be detected without the use of gadolinium-based contrasts using methods including arterial spin labeling (ASL) and IVIM imaging. ASL reports are often limited by the technical implementation of the technique; however, CBF results estimated from ASL may be similarly capable of differentiating among pseudoprogression and true progression as CBF estimated from DSC and may improve DSC diagnostic accuracy in differentiating tumor progression and pseudoprogression.[104,105] Perfusion-related parameters estimated from IVIM, such as maximal IVIM perfusion and minimal diffusion coefficient, were also correlated with patient survival.[106] In the application of MRS, the ratio of Choline (Cho) and N-Acetylaspartate

(NAA) has been correlated to tumor cell density and is often used as a biomarker for detecting tumor and tumor response.[107,108] Large decreases of normalized Cho were correlated with worse median OS and PFS comparing post- and pre-RT data.[109] Another study compared MRS data from pre-RT to data from the third week of treatment; results showed that patients with stable or decreased median or mean Cho/NAA ratio showed less risk of tumor progression than patients presenting increased Cho/NAA ratios over the same period.[110] A recent work proved that CEST asymmetry within the CTV prior to fractionated IMRT was significantly higher in the GBM patients with early progression, suggesting the value of CEST in GBM patient stratification.[111]

In the differentiation of radiation-related necrosis from tumor recurrence, lower mean ADC results are often found in recurrent tumors.[112] Peritumoral ADC results have also been correlated to tumor recurrence.[113] In contrast, radiation necrosis is often characterized by spotty and marked hypo-intensity lesions with higher maximal ADC values.[114] DCE-MRI has demonstrated that higher K^{trans} and CA concentration AUC are more reported in recurrent gliomas than pseudoprogression and radiation necrosis.[115,116] CBV results from ASL have been reported with improved performance than DSC results in distinguishing radiation necrosis from recurrent tumor; in regions presenting mixed radiation necrosis, DSC could fail on estimating true blood volume due to leakage artifacts.[117] A nearly doubled Cho/NAA ratio in MRS has been reported in recurrent tumors in comparison with radiation necrosis (2.72 vs 1.46, $p < 0.01$).[118] Higher concentrations of Cho and Cr correlated with low lipid and lactate were also associated with necrosis in high-grade tumors,[119] but reduced Cho and Cr levels were correlated to radiation necrosis in post-radiosurgery MRS data of patients with brain metastasis.[120] Some works have demonstrated improved accuracy for differentiating recurrent tumor from radiation necrosis or pseudoprogression via combinations of different qMRI metrics. A study of 70 patients demonstrated diagnostic accuracy for distinguishing radiation necrosis from tumor recurrence by rCBV, K^{trans} and ADC individually was 85.8%, 75.5%, and 71.3%, respectively, while the combination of rCBV and K^{trans} as a multiparametric approach improved the overall diagnostic accuracy to 92.8%.[121] Similarly, another 35 patients study showed that the combination of rCBV and ADC improved AUC from 0.801 for a single modality to 0.877 in tumor progression prediction versus pseudoprogression.[122] Combined MRS and DSC result, also outperformed DSC alone in recurrent tumor detection.[123] When DCE-MRI, DWI, and MRS scans were all combined, the accuracy of recurrent tumor detection against radiation necrosis could be as high as nearly 97%.[124]

As computational imaging biomarkers, radiomic features extracted from multiple MRI modalities can be integrated into mpMRI analysis workflow; these quantitative results could further improve recurrent tumor detection accuracy. As an example, a model incorporating radiomic features from DWI and DCE-MRI outperformed both individual MRI metrics and radiomics approaches based on individual MRI modalities.[125] A challenge with such modeling is feature selection, which determines the best parameter subset from a large number of parameters in prediction results. This step is crucial in RT assessment with a limited overall sample size. Machine learning techniques and the recently investigated deep learning techniques may provide novel tools for non-explicit modeling. Based on rCBV and CBF, AUC for radiation necrosis and recurrent tumor detection could be as high as

0.94 using the supporting vector machine method.[126] In true progression/pseudoprogression differentiation, long short term memory (LSTM) neural network achieved AUC values 0.64, 0.69, and 0.81 using 3, 5, and 7 MRI modalities, respectively.[127]

3.2 | Breast

Breast cancer is one of the most common cancers and the main cause of death in women all over the world. Mammography, digital breast tomosynthesis, ultrasound, and MRI are well-established clinical imaging modalities for the diagnosis of breast lesions, which are known to reveal different aspects, and provide complementary information for improved accuracy. Breast MRI is considered the most accurate for evaluating the extent of the disease, which is very important for determining treatment strategies, including surgery (lumpectomy, mastectomy, axillary dissection), chemotherapy (neoadjuvant or adjuvant), and RT (intra-operative or post-operative). DCE-MRI can assess tumor angiogenesis and vascular properties, which is the current standard used for the diagnosis of breast lesions and the essential imaging sequence required in the mpMRI protocol. DWI can assess tumor cellularity, which can provide a non-contrast-based MIR imaging method for the characterization of breast lesions, and is shown to have diagnostic value to differentiate between benign and malignant lesions. Taken together, mpMRI for breast cancer needs to include DCE-MRI with pre- and several post-contrast T1-weighetd images, and optional T2-weighted and DWI images.[128] The current standard of care for women diagnosed with early stage breast cancer is breast-conserving surgery (BCS) followed by external beam RT, commonly delivered over 3–6 weeks. For patients receiving mastectomy, preoperative MRI can provide important information for evaluating the involvement of chest wall muscle and the axillary lymph nodes, to determine the coverage of the post-operation RT.

In the last two decades, neoadjuvant chemotherapy given before surgery has become a very important treatment modality. Very effective chemotherapy and targeted therapy regimens are available and many patients can achieve pathology complete response (pCR), which raises a question about the optimal surgery and RT protocol that can be offered to a patient following neoadjuvant therapy. However, previous studies in patients who showed a complete clinical remission found a higher locoregional recurrence rate in the no surgery group compared to the surgery group,[129] and more research is needed. Longitudinal MRI performed during neoadjuvant chemotherapy may be performed to monitor the response, as shown in Figure 4. The knowledge of the response in primary cancer and axillary lymph nodes can be used for choosing the optimal management strategy, including change in therapy regimen, timing and type of surgery, and post-operation RT coverage. It is known that while the accuracy is very high in mass lesions that show concentric shrinkage, MRI may miss residual presenting as scattered cells in non-mass lesions (e.g., lobular cancer and cancers with extensive intra-ductal component or ductal carcinoma in situ).[130] Many studies have also reported that the diagnostic accuracy of MRI is dependent on the molecular subtype,[130-132] but a large sample size is needed to evaluate the accuracy of MRI in predicting pCR in each subtype. Only when the negative predicting value (NPV) is approaching 100% (that is, the false-negative rate is extremely low) the patient can be confidently treated with radiation alone without surgery. The same strategy has been implemented for the management of axillary nodes.[133,134]

With the success of neoadjuvant chemotherapy that has become a very important treatment modality, neoadjuvant RT has also been offered to patients in a clinical trial setting. Similarly, this may be used to ablate the tumor and facilitate surgery, or to provide local control to allow delayed surgery, or even further, to avoid surgery completely. In the last decade, the accelerated partial breast irradiation (APBI) has gradually evolved as an alternative option for whole breast irradiation following breast-conserving surgery in low-risk patients with early stage disease. APBI is featured by higher doses of radiation in fewer fractions. One approach is that patients can undergo intra-operative RT (IORT) at the time of breast-conserving surgery. Preoperative bilateral breast MRI can detect occult lesions in the ipsilateral and contralateral breasts, and provide a valuable tool in the proper selection of patients best 6suited for IORT.[135-137] Even in highly selected, favorable risk patients, MRI-detected additional lesions may change surgical and RT recommendations in a substantial percentage of patients.[135] Another approach of APBI is pre-operative delivery of external beam irradiation in a single or fractionation delivery. mpMRI can be used to delineate small target volumes and monitor treatment response. In an investigation of single fraction partial breast SBRT, mpMRI including DCE-MRI PK parameters and DWI ADC were studied to monitor radiation effect (Figure 5). The relative change in reference to the pre-treatment value of DCE-MRI K^{trans} in PTV and ADC in GTV were linearly correlated with dose level.[138] In another study of neoadjuvant SBRT, the changes in DCE-MRI single enhancement and PK parameters were different in three different patient groups with different fractionation regimes; MRI exams performed at 1 week post-RT maybe too early for a reliable response assessment.[139] In a proposed prospective clinical trial to test MRI-guided ablative APBI,[140] multiple MRI exams were scheduled as single-fraction radiation delivery follow-ups before breast-conserving surgeries. It was concluded that neoadjuvant partial breast irradiation might provide a feasible alternative to standard post-operative irradiation, and could even result in postponement or omission of surgery if pCR can be accurately predicted in selected low-risk patients.[141]

Machine learning modeling is increasingly being employed to generate models of breast chemo-RT prediction that includes mpMRI and other radiographic measurements. In a representative work, disease-specific survival in breast cancer was correlated with mpMRI changes before and 2 weeks after the start of neoadjuvant chemo-RT—specifically lesion size, volume distribution and mean plasma how in DCE-MRI, and maximum ADC in DWI.[142] A limitation of existing machine learning work is the potentially suboptimal statistical power limited study sample sizes, which are frequently limited by their single-institution nature and the need for additional scans or image protocols that are not considered standard of care for that disease site. Nevertheless, mpMRI studies using relatively larger patient cohort sizes have been reported. As an example, a large retrospective series of 586 women from four centers used radiomics of mpMRI before the start of neoadjuvant chemo-RT in breast cancer to build a model to predict pCR with AUC 0.86.[143] The drawback of such studies is that multi-institution acquisitions are often performed with various acquisition parameters, which can alter imaging appearance and compromise the analysis.

3.3 | Prostate

MRI better visualizes the prostate and relevant pathology as compared to other imaging modalities due to its high soft-tissue contrast, high resolution, and the ability to obtain tissue function metrics from its diverse contrast mechanisms. The radiology community has utilized MRI for the noninvasive assessment of the prostate since the 1980s and has embraced the use of the mpMRI in its diagnosis and staging of prostate cancer. This process is formalized in the PI-RADS system.[54] The diverse contrast mechanisms of MRI and the functional techniques such as DCE-MRI, DWI, and occasionally MRS, as well as anatomical MRI sequences, have led to te improved detection of prostate cancer thereby increasing confidence in the detection of benign diseases and accurate tumor localization. This accurate localization allows for MRI-targeted prostate biopsies which facilitate the pathological confirmation of lesions detected by mpMRI and lead to improved detection of prostate cancer.[144] In the radiation oncology setting, mpMRI is utilized differently than the diagnosis and staging focus of radiology. The precise delineation of the prostate, other target structures, and organs at risk is of paramount importance for accurate RT and properly acquired mpMRI can facilitate the delineation of the prostate and other structures. Additionally, radiation dose escalation has shown to increase tumor control[145] and some groups are utilizing mpMRI to delineate the dominant lesions within the prostate to target these lesions for higher levels of dose with the hope of increased tumor control without increasing side effects.[146-148]

Although modern treatment of prostate cancer has resulted in improvements in both tumor control and reduced toxicity, there are still a meaningful number of patients that suffer from both lack of local control and toxicity. mpMRI, in conjunction with other pathological and diagnostic assessments, has the potential to stratify risk prior to therapy, and possibly predict treatment response, making individualized dose prescriptions a possibility. The ability to evaluate a patient's response to RT during the treatment course may be able to improve both tumor control and reduction of toxicities by adapting the remaining treatments to either boost the areas that are not effectively responding or reducing radiation dose, thus sparing the OARs if the tumor is responding robustly. Alternatively, if the response to the RT can be evaluated soon after the completion of the treatment course, and the probability of control and recurrence can be effectively estimated, then personalized follow-up assessments can be implemented.

mpMRI of the prostate utilizes several different pulse sequences to characterize the prostate: T2-weighted (T2w) sequences, DWI, DCE-MRI, and sometimes MRS. T2w sequences exhibit the prostate zonal anatomy end surrounding relevant anatomy as well. Peripheral zone (PZ) tumors typically appear as hypointense lesions on T2w images, but other conditions can also exhibit this appearance: prostatitis, hemorrhage, etc. Tumors in the transition zone (TZ) can be difficult to visualize on T2w images due to the heterogeneity of hyperintense glandular tissue and hypointense stromal tissue that comprises the TZ. ADC images that are generated from DWI use the water diffusion properties of the tissue as an endogenous contrast mechanism making it quite effective at prostate cancer detection and a good candidate as a biomarker for treatment response metrics. High-grade prostate cancer tumors often exhibit hypercellularity, more dense packing of cells, as compared to

the surrounding tissue. This hypercellularity restricts the diffusion of water and appears hyperintense on DWI images and hypointense on ADC images.

In general, increased diffusion from ADC results is noted during RT[149,150]; after RT, reduced diffusion is noted in locally recurrent prostate cancer, which adds significant accuracy to the detection of recurrent prostate cancer compared to T2-weighted imaging alone.[151,152] In a study of low and intermediate-risk localized prostate cancer,[153] the study collected serial mpMRI acquisitions at weeks 0, 2, 4, 6, and 8 in patients with low and intermediate-risk localized prostate cancer. Repeat mpMRI datasets were also collected in volunteers to quantify T2w and ADC metric variations in individuals not undergoing RT. The imaging responses were compared and were correlated against pathological metrics, PSA levels, and clinical staging. In the central gland (CG) the ADC values elevated significantly from baseline; for the peripheral zone (PZ), there was a trend of reduced ADC but significance was not achieved. The tumor had a strong ADC response with an approximate 14% increase at week 6. In the CG there was a 5% increase in T2 at week 2, but then returned to baseline at later time points. The PZ demonstrated a significant decline of 23% at week 6 and 26% at week 8. The tumor T2 responses varied widely between patients and non-significant were reported at weeks 4 and 8. In short, the ADC was more robustly affected from RT for the entire prostate and central gland, while the peripheral zone changes were best detected using T2 with the tumor demonstrating the largest changes in ADC. These ADC and T2 results were also correlated with follow-up PSA measurements; baseline PSA, nadir PSA, and 1-year PSA response velocity were analyzed. Baseline PSA nadir and PSA were uncorrelated with both baseline and biweekly ADC and T2 values. The 1-year PSA response velocity was significantly correlated with tumor baseline T2 response at week 6. In another study of hypoFLAME trial that involves ultra-hypo fractionated RT, 47 patients with biopsy-proven, clinically localized, intermediate to high-risk prostate cancer were studied.[154] Twenty-eight of the 47 patients received hormonal therapy (HT) concurrent with RT. For the CG, a median decrease of 12% on T2 maps and 8% on ADC values were seen in patients that underwent HT at week 5. These values were significantly lower than pretreatment values. For patients that did not undergo HT, there were no significant differences, only a slight decrease in ADC was reported. The PZ demonstrated a decrease of 17% in T2-values and 18% in ADC-values in patients that received HT, while patients that did not receive HT showed no significant differences, only a slight ADC decrease. The tumor displayed no significant increases in both T2 and ADC, 5% and 7%, respectively, for patients that received HT, but for those without HT the ADC had an increase of 20%, which was significant. Radiomics features from T2w and ADC images were also studied for RT response assessment.

DCE-MRI is sensitive to the vascular microenvironment differences between tissues. Prostate cancer tumors are thought to have increased angiogenesis, which increases the number of vessels, and these vessels have higher permeability than normal vessels; this manifests as earlier and more pronounced enhancement on dynamic T1w image than normal prostate tissue. The sensitivity of DCE techniques to the tissue vasculature also makes it a strong candidate as a biomarker for prostate treatment response. In general, increased blood perfusion results from DCE-MRI have been observed after prostate RT.[149] In a study of small patient cohort size with pre-RT and multiple post-RT exams,[155] the DCE-MRI

perfusion rate increased significantly at the immediate post-RT time point in reference to the pre-treatment baselines. At the 1-year post-treatment time point, the perfusion rate dropped below pre-treatment values. Normal prostatic tissue experienced a similar outcome with increased perfusion rate from pre-treatment to the immediate post-treatment time point followed by a drop at 1-year post-treatment time points. The blood volume metric followed a similar dynamic as the perfusion rate for both cancerous and normal prostatic tissue. A decline in blood volume at the 3-month and 1-year post-treatment time points were observed, but this decrease was significant for cancerous tissue and not for normal prostatic tissue; inversely, the extraction coefficient in cancerous prostatic tissue decreased immediately after RT, then increased at 3-month and ultimately at the 1-year time point. In contrast, normal prostate tissues behaved opposite in extraction coefficient dynamics, but significant differences between cancerous and normal prostatic tissue were found at the pre-treatment time point only. DCE-MRI perfusion metrics have also been reported together with ADC results in mpMRI protocol design. In another longitudinal study of prostate cancer RT,[148] an increase in ADC and v_e (volume fraction of the EES in Tofts model) were demonstrated. These changes were hypothesized to be due to the decrease in cellular density. Additionally, a substantial and persistent increase in v_e showed in the normal-appearing TZ following RT.

Radiomics and machine learning are promising and powerful tools that can analyze these large dynamic datasets and discover patterns and correlations efficiently, potentially automating the process.[156] In a pilot study of 93 patients with paired pre- and post-IMRT MRI exams,[157] RT response was determined by changes in ADC value, and 45% percent of patients were classified as responders. Two radiomic features of T2 images and 15 features of ADC images demonstrated significance between responders and non-responders. Also, cross-combined T2 and ADC predictive radiomic models were analyzed; the pre-T2 model, post-T2 model, and pre-ADC model all showed high predictive value. However, there have been very limited studies that have correlated the dynamic mpMRI changes in radiomics with long-term treatment outcomes or toxicities. With further study, mpMRI with radiomics analysis may be able to predict treatment response, while in the early treatment phase, shifting the current paradigm and reducing recurrence.

3.4 | Head and neck

As reported by the American Cancer Society, about 50,000 new cases of head and neck cancer (HNC) are diagnosed each year in the United States.[158] Generally, HNC originates from mucosal epithelia of the oral cavity, larynx, and pharynx, often linked to the use of tobacco and consumption of alcohol.[159,160] The majority of these patients present with locally advanced, non-metastatic disease, most of which receive RT and possibly concurrent chemotherapy, which provides an additional survival benefit compared to RT alone at the cost of an increase of treatment morbidity.[161] Currently, the anatomically based tumor, node, metastasis (TNM) staging system is utilized to categorize tumors of the head and neck region, and provides prognostic information, which guides therapeutic decisions in HNC management. However, the TNM based staging system has significant deficiencies. More specifically, patients with the same stage of disease often exhibit different outcomes in response to identical treatments. This implies that the standard approach of offering more

intensive therapy to the patients of the same TNM stage significantly increases the risk of toxicity for all the patients while providing benefits for only a small proportion of the patient population. With additional physiologic and biologic prognostic factors, mpMRI has been adopted to augment the tumor information provided by the TNM staging system in RT practice. Figure 6 illustrates an example of DWI application in HNC IMRT target delineation.

In addition to the consideration of tumor, the role of normal tissue should not be neglected in HNC management. This is particularly important in HNC since standard treatment could eradicate the disease in the majority of HNC patients with locally advanced, non-metastatic disease, but cause severe side effects including severe short-term mucositis, dental disease, chronic swallowing dysfunction, and permanent xerostomia, as a result of radiation-induced injury to the salivary glands. Advances in RT technologies (including IMRT and IGRT) allows for the sparing of the parotid glands and as such reduces the risk of permanent xerostomia, a debilitating adverse complication of RT. Currently, parotid tolerance in RT is based on radiation dose and the volume of irradiated tissue, which correlates parotid gland mean dose with subsequent salivary production.[162] It has been reported that the recovery probability of saliva production is significantly declined when the parotid gland mean dose is >26 Gy.[163,164] However, it has also been found that individual patient response to therapy varies, with reported subjective xerostomia even after parotid-sparing RT.[165] This manifests the limit that the physiologic basis for the relationship between the radiation dose to the parotid and reduced saliva production is not well understood. mpMRI might provide valuable functional information on potential changes in parotid physiology and as such enhance the ability to predict the development and severity of radiation-induced xerostomia, leading to more individualized treatment.

Many studies were carried out to predict or assess the RT response of HNC using mpMRI, while DWI has been more commonly studied. In a representative study of chemo-RT assessment, two post-treatment DWI scans were analyzed in reference to the pre-treatment baselines.[166] The study reported that the pre-treatment baseline ADC value in neck lymph nodes was significantly lower in complete responders (CR) than it was in partial responders. A statistically significant increase of ADC value was observed in complete responders after one week of treatment. Both pre-treatment ADC value and change in ADC within the first week of chemo-RT demonstrated great value in the prediction of treatment response with relatively high sensitivity and specificity. DWI has also been investigated to monitor normal tissue injury of RT. A study of parotid gland evaluation with DWI reported that after IMRT delivery, mean ADC in the ipsilateral, unspared glands (mean dose: 39.2–69.3 Gy) increased while that in the contralateral parotids (mean dose: 16.2–25.1 Gy) remained unchanged in reference to the pre-treatment baselines.[167] Radiomics features derived from DWI may add values in monitoring treatment response. In a study of HNC chemo-RT with radiomics analysis of T2w and DWI images, while pre-treatment ADC had a high predictive accuracy of 80% (sensitivity 54.5%, specificity 94.7%) in predicting regional failure of lymph nodes, a combined model using both ADC and its radiomic features improved prediction accuracy to 82.8% (sensitivity 63.6%, specificity 94.4%).[168]

In addition to DWI, other qMRI methods have been incorporated in mpMRI protocols for HNC RT assessment. In a study of locally advanced HNC, mpMRI (DWI and DCE-MRI) was adopted jointly with ^{18}FDG-PET to monitor treatment response.[169] A significantly greater initial slope of the CA uptake curve was found in patients with locally controlled lesions. In contrast, patients with locoregional recurrence developed in the primary tumors and lymph nodes had significantly lower ADC values during and after the RT course. In another study with a similar imaging protocol design (mpMRI + ^{18}FDG-PET), primary tumor k_{ep} and nodal region v_e calculated from the Tofts model were found to be independent prognosticators of oropharyngeal/hypopharyngeal squamous cell carcinoma in terms of 3-year progression-free survival (PFS) and overall survival (OS) rates.[170] The joint use of DCE-MRI with ^{1}H-MRS and ^{18}FDG-PET also demonstrated complementary, not competitive, in tumor metabolism and perfusion evaluation at the 3–4 month post-treatment time point.[171] Additionally, feasibility also demonstrated a statistically significant correlation between T1ρ value increase and parotid volume atrophy rate after RT completion.[172]

3.5 | Rectum

Response assessment of rectal cancer is of particular interest due to reported considerable outcome variations in chemo-RT.[173] mpMRI has been evaluated extensively as a predictor of neoadjuvant chemo-RT response in patients with locally advanced rectal cancer, as patients with complete clinical and pathologic response may be able to forego surgery which typically results in temporary or permanent colostomy.

Diffusion weighted imaging has been a dominant quantitative MRI method in studies.[174] As an example, Figure 7 shows a mpMRI analysis of locally advanced rectal cancer using DWI and T2-weighted MRI. Several studies have reported that higher tumor mean ADC values were found in patients with better response after chemo-RT of locally advanced rectal cancer,[174-177] and ADC results had good correlations with pathology results.[178,179] ADC was also found in good accordance with T2w MRI in chemo-RT outcome prediction performance, while the joint use of ADC and T2-weighted MRI results showed improved AUC results as compared to mono-modality results.[180-182] Additionally, tumor volume measurement on DWI images was also reported as a good indicator of chemo-RT response.[183]

When DCE-MRI was examined, a larger K^{trans} decrease after treatment was associated with good response after chemo-RT[184-187]; lower K^{trans} and k_{ep} in post-treatment DCE scans were also reported in complete response patients.[188] DCE-MRI images were also good indicators in good correlations with pathology results.[189,190] Following fast imaging basis in DCE-MRI, a dynamic T1 mapping study showed significant differences of tumor microcirculation measure between responders and nonresponders groups after rectal carcinoma chemo-RT.[191]

While changes in one qMRI obtained during chemo-RT can achieve good accuracy in predicting pathologic complete response (pCR) found at surgery,[173,192] more recent works utilized sophisticated data modeling methods for analysis leading to multiparametric models. As an example, regional mean values of enhancement ratio from DCE-MRI and ADC from

DWI in combination with radiomics features were found as the best discrimination of rectal cancer pathologic response compared to pre-treatment alone, single time point analysis, and convolutional neural network analysis.[12] An additional recent study also reported the best discrimination of pathologic response with pre- and post-chemo-RT images based on a decision tree analysis of perfusion and diffusion-based metrics.[193] Of note, mpMRI has been studied together with PET-CT for monitoring chemo-RT patient outcomes. However, ^{18}FDG-PET demonstrated limited benefit in data analysis when the joint use of DWI and T2w images have demonstrated better detectability.[194,195]

3.6 | Others

MRI has found its critical role in RT of gynecology cancerous malignancy,[196] and mpMRI has been commonly studied for cervical cancer RT response assessment. A collection of studies reported increased tumor mean ADC values[197-200] and decreased K^{trans} values[197,198,200] after chemo-RT. DWI and DCE-MRI results have also demonstrated significant differences between different responsive groups.[201] In an IVIM analysis of DWI, the changes in diffusion coefficient D and perfusion-related diffusion fraction F were related to tumor shrinkage during the treatment course.[202] In a mpMRI study with BOLD-MRI and ^{1}H-MRS, recurrent lesions after cervix carcinoma treatment showed higher R2* levels as a suggestion of higher concentration of Hb, and significantly elevated choline in ^{1}H-MRS choline-containing resonance (tCho) analysis was reported.[203]

Lung is a common site of RT application. In monitoring lung cancer RT response, because of sharp contrasts between lung target volume and surrounding normal lung tissue, ionizing imaging methods of CT and PET are commonly used. With their sensitivity to oxygen content, BOLD-MRI/TOLD-MRI can be applied to assess post-RT lung tissue. In a pilot study using a subcutaneous rat model with human lung cancer xenografts, tumor T2* from TOLD-MRI significantly decreased due to post-SBRT impaired vascular oxygenation.[204] As for DCE-MRI application, tumor regression rate was found to be +/− correlated with K^{trans}/v_e after concurrent chemo-RT of NSCLC.[205] In another NSCLS SBRT assessment study, percent changes in K^{trans} and k_{ep} 6-week after radiation were correlated with tumor size reduction in 3-month CT follow-ups.[206]

Liver is another common site for RT. Radiation-induced liver toxicity is a major factor in RT regime design.[207] A unique aspect of the liver is its two-phase perfusion model, arterial phase, and portal phase. While liver is considered as a single compartment, it receives blood inflows from the hepatic artery and portal vein.[208] Thus, DCE-MRI has been studied to investigate liver perfusion evolution after RT. As a non-compartmental model parameter, portal venous perfusion map has been reported as a good predictor of indocyanine green (ICG) clearance rates (overall liver function biomarker)[209] and a key parameter in liver SBRT normal tissue complication probability (NTCP) modeling.[210] Biological subvolumes from arterial perfusion demonstrated significant differences between progressed and non-progressed tumors after RT.[209] DWI has been reported for assessing yttrium-90-labeled microspheres treatment of unresectable hepatocellular carcinoma (HCC): increased tumor ADC results after yttrium-90 ablation were reported earlier than morphological changes.[211,112] When IVIM was analyzed, diffusion coefficients in regressive tumors were

found to be higher prior to yttrium-90 ablation; v_e in DCE-MRI was reported with increased values, which supplements the indication of reduced cellular density by ADC results.[213]

While PET imaging used as in PET-CT or PET-MRI has been commonly used in pancreatic oncology,[214] limited works have reported mpMRI investigation for pancreatic RT. In neoadjuvant chemo-RT for pancreatic ductal adenocarcinoma (PDAC), tumors with a low ADC mean value in DWI at baseline responded poorly to the standard treatment.[215] In a comparison study that investigated six DWI models, all models' parameters were able to identify treatment effect.[216] However, DWI was reported with no conclusive advantages over FDG-PET in some studies.[217] In a preclinical study, tumor K^{trans} and k_{ep} from DCE-MRI significantly decreased after I-125 seeds brachytherapy of PDAC xenografts in a murine model.[218] Tumor T2 value was demonstrated with early radiation effect capture in another experiment of small animals with PDAC disease model.[219]

Similarly, mpMRI investigation for esophageal RT assessment is limited. In a study of esophageal squamous cell carcinoma (SCC) chemo-RT, DWI ADC was used to identify significant survival rate difference.[220] another study using both DCE-MRI and DWI, K^{trans} and k_{ep} acquired in the middle of the RT course captured significant differences between different responsive groups, but ADC only indicated such difference in pre-treatment results.[221] Another study reported that a90% percentile change in CA concentration AUC could predict pathologic complete response after neoadjuvant chemo-RT.[222] In a T1 mapping study assessing cardiac toxicity after esophagus chemo-RT, pre-CA T1 value of myocardium increased 6 months after treatment, which was earlier than late CA enhancement results that demonstrated significant results 18 months after treatment.[223]

Pilot works of mpMRI in sarcoma evaluation have been reported. In a study of retroperitoneal sarcoma pre-operative RT, tumor median ADC was found with a significant increase after RT, and both ADC and diffusion coefficient D from IVIM were correlated with histopathological cellularity.[224] In an evaluation of spine metastatic sarcoma SBRT, tumor mean/max of K^{trans} and v_p significantly decreased in post-treatment DCE-MRI. A simple score system from DCE-MRI results achieved 100% accuracy in local control prediction.[225]

4 | CHALLENGES AND LIMITS

Although many mpMRI techniques have been extensively reported in clinical investigations, challenges and limits exist and may potentially cause obstacles in its adoption into clinical practice. In the following section, these challenges and limits are to be discussed.

4.1 | Standardization of acquisition and processing of mpMRI data

As demonstrated in the previous sections, mpMRI is used to assess treatment response of RT for numerous diseases; however, the large site-to-site variation of data acquisition methods (including imaging protocols and scanners) and data processing methods (including quantitative parameter calculation, tissue segmentation, and radiomics feature extraction) may compromise the reproducibility and repeatability of mpMRI data. The data reproducibility is generally defined by the closeness of agreement between measured

values obtained by replicate measurements using different acquisition conditions[226]; these conditions may include different sequence parameters, scanners, and non-scanning protocol parameters (such as CA injection rate in DCE-MRI). Likewise, data repeatability is defined as the closeness of agreement between measured values obtained by replicate measurements performed on the same scanner, with identical imaging acquisition protocols.[227] The data repeatability is mainly affected by image data analysis, which may include quantitative model selection, raw data pre-processing, and parametric data post-processing.[228]

To address reproducibility and repeatability, several initiatives were proposed, including Quantitative Imaging Biomarker Alliance (QIBA) by Radiological Society of North America (RSNA), Quantitative Imaging Network (QIN), and Reference Image Database to Evaluate Therapy Response (RIDER) by National Center Institute (NCI), and European Imaging Biomarkers Alliance (EIBALL) by European Society of Radiology (ESR). As an example, QIBA provides templates to record and organize data reporting along with available protocol recommendations addressing reproducibility and repeatability.[229] To develop prospective multi-institutional mpMRI clinical trial, the standardization of acquisition and processing is crucial to enable data analysis and interpretation across different institutions.

Another challenge of RT assessment using mpMRI is the variation of RT implementation. In the last two decades, RT delivery techniques have undergone rapid progress from 3D-CRT to IMRT, volumetric-modulated arc radiotherapy (VMAT), and charged particle therapy using protons and heavy-ion particles. Meanwhile, radiobiological advancements enable novel RT regimens such as SBRT and recent FLASH RT. It is important to acknowledge the importance of RT consistency in the study sample cohort. Although the majority of studies of mpMRI reported homogeneous RT protocols with some acceptable variations, it is challenging to combine different study groups together with consistent mpMRI protocols but different RT protocols. Some radiological theories, such as biological effective dose (BED),[230] provide some solutions to “normalize” RT effects; however, the validity of such approach is not fully understood with limitations in radiobiological theories.[231] When a research protocol of mpMRI in RT assessment is proposed, the consistency of RT protocol should be considered.

4.2 | Data access

Access to proper data is always important for mpMRI methodology development and validation. For most mpMRI studies reported by single institution investigations, the typical patient cohort size ranges from a few samples to a few dozens of samples. In addition to the data reproducibility issue, restricted data access under the current institutional regulation regime also imposes challenges in combining data sample cohorts for mpMRI studies. Although some open databases with mpMRI, such as Quantitative Imaging Data Warehouse (QIDW) by QIBA and The Cancer Imaging Archive (TCIA), have been available to researchers; however, the overall useable samples are still limited. In the era of big data application in medicine, access to high-quality data is crucial to meaningful research and is the cornerstone for the future development of mpMRI in RT.

n addition to mpMRI data, other clinical data are also valuable in assessing treatment response of RT, which include, but are not limited to, imaging metadata, medical records,

and pathology-related information. Among the data, imaging metadata are particularly important and should never be undervalued, given the fact that imaging metadata includes the information on image generation as well as annotations regarding diagnostic, anatomical or pathological details from clinicians. To adequately utilize mpMRI patient data for treatment response assessment, imaging metadata and other medical details (including treatment history, dose regimen, and treatment schedule) should be combined with mpMRI to establish a predictive model for treatment response. Given the limit that the imaging metadata are often stored separately from the imaging data, it is critical, but challenging, to adopt the consistent and standardized naming convention, file organization, and data anonymization and sharing procedures across various institutions on a national or international scale.[232]

4.3 | Clinical interpretations

When interpreting functional parameters from mpMRI analysis, it is important to consider physiological assumptions in the associated microenvironment. For example, the parameter K^{trans} that describes tissue microvessel permeability are commonly derived by Tofts models in DCE-MRI. The elegant two-compartment model design assumes infinite transcytolemmal water exchange, which may not be true, particularly with high CA concentration.[233] Comparison studies showed that K^{trans} derived with and without infinite transcytolemmal water exchange assumptions had different performances in capturing anti-vascular treatment effect.[234] Understanding the limitations of physiological assumptions is also critical in optimizing a data analysis method. Similarly, in a DWI study using different b values, when high b values were used as acquisition parameters for imaging, results indicated extra pathology results and suggested different modeling for more adequate interpretation.[235] One should also be cautious when analyzing mpMRI results derived with different main magnet field strengths. Currently, both 1.5 T and 3 T strengths are dominant selections for clinical MR scanners, while 7 T scanners for cranial imaging have become available. Prior studies revealed that while certain mpMRI parameters might be insensitive to field strength selection,[236] some mpMRI results using different main field strengths may lead to different medical intrepreations.[237] Additionally, when describing the same physiological concept, discrepant information may come from different imaging modalities. While DSC has been recognized for its role in acute stroke treatment, noticeable discrepancies of cerebral blood flow and cerebral blood volume were reported between DSC and ^{15}O-water PET measurements.[238,239] Thus, when reporting results from mpMRI, it is important to clarify the corresponding assumptions and the associated limitations.

It is also important to understand the uncertainties of derived functional parameters in clinical use. The uncertainties might arise from both physical variations in technical implementations and biological variations with in vivo data. More specifically, in DCE-MRI, the uncertainties in deriving K^{trans} may come from T1 measurement, CA injection, and PK model fitting. Although these physical uncertainties cannot be fully eliminated, they need to be characterized in a controlled condition, preferably in repetitive phantom experiments, for potential uncertainty reduction.[240,241] Moreover, biological uncertainties are inherent and are very challenging to manage in a clinical setup. AIF, the dynamics of CA in major blood vessels, is a key factor in the PK model solution. However, the blood dynamics in the human

body are affected by many factors and often are not constant, and experiments have shown intra-patient AIF variations on different days.[242] Although, the use of population-averaged AIF with known parameters can eliminate intra-patient variations, but this approach ignores the larger inter-patient blood dynamics variations, which may lead to reduced precision in cross-patient comparison studies.[243] Furthermore, the intra-patient variation in biology may affect, and even compromise, the results in paired mpMRI imaging studies for pre-treatment and post-treatment evaluation. Currently, quantitative parameter value changes (post-treatment–pre-treatment) have been extensively reported in the mpMRI applications of RT assessment. The repeated scans, both pre- and post-treatment, are favored to minimize intra-patient biological variations to reveal the treatment-induced changes; however, this requires extensive care and imposes logistic challenges.

4.4 | Integration with RT workflow

There are some additional challenges to integrate mpMRI into the RT workflow for treatment response assessment. One particular challenge is the requirement of high spatial integrity, which is crucial in treatment target definition and localization. In modern RT featured by high precision radiation delivery, image localization may need 1 mm or less spatial accuracy.[244] Some mpMRI techniques, such as echo-planner acquisition in DWI, may suffer significant geometrical distortion issues.[14,245] A second challenge is the requirement of high image resolution. Due to limited scan time, many mpMRI acquisitions cannot reach a high image resolution, as is achieved in typical CT simulation image volumes, which could be a problem using regions-of-interest defined by mpMRI in the RT workflow.[246] Additionally, it may be challenging to register low-resolution mpMRI images to high-resolution images for RT planning; it generally is recommended that high-resolution anatomical MRI data share the same coordinate space with mpMRI scans to enhance registration accuracy.

Another challenge is to determine the optimal timing for mpMRI during the RT course. In a regular fractionated treatment course that may last up to 7 to 8 weeks, RT variations that include patient-specific morphological changes in patient anatomy and biological variation caused by cell phenotypic changes may occur, and these variations cannot be managed by pre-RT imaging and planning alone.[247] Adaptive RT evaluates the intra-course patient variations and generates possible revised RT plans as a feedback control strategy.With pre-RT acquisition, intra-course mpMRI exams can provide biological evaluations for adaptive RT planning strategy.Many studies have shown that mpMRI can capture prominent physiological changes earlier than anatomical variations.[248-251] Nevertheless, the optimal time point for mpMRI during the RT course is difficult to define[252]; such definition needs extensive in vivo comparative studies with different mpMRI exam frequencies utilizing the same RT protocol. Additionally, early RT adaptation without observed patient anatomical changes is too immature to be a clinical practice with consensus, and thus more future investigations are warranted.

In addition, there are various logistic challenges in mpMRI implementation in Radiation Oncology clinics. mpMRI data, such as high temporal resolution DCE-MRI, can be very large in terms of data size. When using such imaging data within the radiation oncology

information system (ROIS), data transfer and loading efficiency can be a potential problem. Also, the currently available imaging viewers in ROIS do not have a full toolbox of functions for mpMRI analysis. When transferring image-based mpMRI analysis results, such as segmentation contours, from self-developed or pre-clinical mpMRI analysis tools to ROIS, special quality assurance tests should be conducted to ensure data integrity.[253] Registrations of mpMRI image volumes acquired by a standard diagnostic MRI scanner with curved couch tops to RT imaging volumes acquired with flat couch tops in radiation oncology can be a practical challenge.[254] mpMRI exams using radiation oncology-specific scanners, such as MRI simulator and MR-LINAC,[255] might be an appealing option for mpMRI applications in RT response assessment on a large scale; this option requires transferring complicated scanning protocols to radiation oncology clinics and requires substantial validation efforts which optimally would be performed by a qualified imaging physicist that might not be available in a radiation oncology team, although the imaging expertise within a modern radiation oncology department is potentially greater than historical norms and may be sufficient for these tasks.[256] The mpMRI protocols available on radiation oncology scanners may also need validation and optimization to accommodate RT-specific applications.

5 | DISCUSSIONS AND FUTURE DEVELOPMENTS

5.1 | Novel qMRI techniques at ultrahigh field

It is well known that the sensitivity of MRI depends on the signal-to-noise ratio (SNR) of the tissue of interest acquired during scanning. Given the fact that SNR is approximately linearly proportional to the main static magnetic field strength B_0, the performance of mpMRI could be greatly enhanced at ultrahigh magnetic field strength. Compared with conventional scanners, the increase in SNR for ultrahigh field MRI scanners allows for greater spatial and spectral resolutions which may reveal anatomical and pathological findings that were previously undetectable.[257] Furthermore, the wide adoption of ultrahigh MRI scanners (e.g., 7 T whole-body MRI scanners) may enable various novel applications feasible in a typical clinical setting.

Among these MRI techniques, an interesting one is high-resolution quantitative sodium imaging.[258] Angiogenesis and cell division are strongly associated with tumor progression. Changes in sodium concentrations have been demonstrated to be sensitive to cellular proliferation, linked to tumor malignancy.[259] Although sodium (^{11}Na) is the second most abundant magnetic nucleus in a human body next to hydrogen (^{1}H), the sodium concentration is intrinsically low and as such results in low SNR, long scan times, and low spatial resolution. In the past, due to this inherent weakness, the clinical applications of sodium imaging were limited. At ultrahigh magnetic field strength, this limitation may be overcome. It has been recently reported that high-resolution quantitative in vivo sodium imaging was achieved on a 9.4 T MRI scanner.[258]

5.2 | Advanced MRI-RT systems

In the modern era, numerous efforts are gaining momentum by advancing cancer care through individualized treatment. One of the most promising trends is MRI-guided

RT. Currently, several hybrid MRI-guided Radio Therapy (MRgRT) systems have been implemented in clinics: one hybrid system combines a LINAC with a 0.35 T split-bore MRI system (ViewRay, OH, USA); another system combines a LINAC with a 1.5 T closed-bore MRI system (Elekta, Stockholm, Sweden).[260] With the recent clinical adoption of MRgRT, real-time MRI-guided proton beam therapy (MRPT) has been proposed.[261] With potential improvements of MRPT over conventional proton therapy and over x-ray beam therapy, feasibility studies have been conducted on the developments of software and hardware aspects of the proposed MRPT systems.[261,262] Although most of the studies are simulation-based, the early research demonstrated that MRPT is not only conceptually plausible but also practically feasible.

5.3 | Deep learning application in mpMRI

Artificial Intelligence (AI) has become a widely discussed topic in both academia and industrial areas. Being propelled by the growths of mathematical theories and massive computation power, as a representative AI implementation, deep learning (DL) based on artificial neural networks has demonstrated impressive performances in image recognition, language translation, disease diagnosis, tumor segmentation, and other complicated tasks. In mpMRI image analysis, deep learning techniques could extract information from images without an explicit modeling process; the additional information may serve as opportunities to develop novel mpMRI theories. Additionally, automation in deep learning may facilitate the improved integration of mpMRI into the radiation oncology clinic, such as robust automatic contouring and image registration. Potential therapeutic prediction in RT by combining deep learning and mpMRI data is also conceptually promising: with mpMRI acquired prior to RT, DL-based outcome predictions could be available at the treatment planning stage. Guided by these predictions, clinicians could explore alternative treatment plans, such as target definition revision and dose fractionation adjustment, and select a plan that could potentially improve the patient's outcome.[232,252] Furthermore, this strategy could be adopted during a treatment course to optimize adaptive RT. These research and development efforts may pave the way to improved individualized RT.

DATA AVAILABILITY STATEMENT

Data sharing is not applicable to this article as no datasets were generated or analyzed in this review paper.

REFERENCES

1. Boon IS, Lim JS, Yap MH, Yong TPA, Boon CS. Artificial intelligence and soft skills in radiation oncology: data versus wisdom. J Med Imaging Radiat Sci. 2020;51(4):S114–S115. [PubMed: 32859543]
2. Delaney G, Jacob S, Featherstone C, Barton M. The role of radiotherapy in cancer treatment: estimating optimal utilization from a review of evidence-based clinical guidelines. Cancer. 2005;104(6):1129–1137. [PubMed: 16080176]
3. Baskar R, Lee KA, Yeo R, Yeoh K-W. Cancer and radiation therapy: current advances and future directions. Int J Med Sci. 2012;9(3):193. [PubMed: 22408567]
4. Rezai P, Pisaneschi MJ, Feng C, Yaghmai V. A radiologist's guide to treatment response criteria in oncologic imaging: anatomic imaging biomarkers. Am J Roentgenol. 2013;201(2):237–245. [PubMed: 23883205]

5. Eisenhauer EA, Therasse P, Bogaerts J, et al. New response evaluation criteria in solid tumours: revised RECIST guideline (version 1.1). Eur J Cancer. 2009;45(2):228–247. [PubMed: 19097774]
6. Cha KH, Hadjiiski LM, Samala RK, et al. , Bladder cancer segmentation in CT for treatment response assessment: application of deep-learning convolution neural network—a pilot study. Tomography. 2016;2(4):421–429. [PubMed: 28105470]
7. De Salles AA, Gorgulho AA, Pereira JL, McLaughlin N. Intracranial stereotactic radiosurgery: concepts and techniques. Neurosurg Clin. 2013;24(4):491–498.
8. Sneed PK, Suh JH, Goetsch SJ, et al. A multi-institutional review of radiosurgery alone vs. radiosurgery with whole brain radiotherapy as the initial management of brain metastases. Int J Radiat Oncol Biol Phys. 2002;53(3):519–526. [PubMed: 12062592]
9. Lutz W, Winston KR, Maleki N. A system for stereotactic radiosurgery with a linear accelerator. Int J Radiat Oncol Biol Phys. 1988;14(2):373–381. [PubMed: 3276655]
10. Panebianco V, Barchetti F, Sciarra A, et al. Multiparametric magnetic resonance imaging vs. standard care in men being evaluated for prostate cancer: a randomized study. Urologic Oncol Seminars Orig Invest. 2015;33(1):17.e1–17.e7.
11. Petrillo A, Fusco R, Setola SV, et al. Multiparametric MRI for prostate cancer detection: performance in patients with prostate-specific antigen values between 2.5 and 10 ng/mL. J Magn Reson Imaging. 2014;39(5):1206–1212. [PubMed: 25006636]
12. Shi L, Zhang Y, Nie KE, et al. Machine learning for prediction of chemoradiation therapy response in rectal cancer using pre-treatment and mid-radiation multi-parametric MRI. Magn Reson Imaging. 2019;61:33–40. [PubMed: 31059768]
13. Choyke PL, Dwyer AJ, Knopp MV. Functional tumor imaging with dynamic contrast-enhanced magnetic resonance imaging. J Magn Reson Imaging Off J Int Soc Magn Res Med. 2003;17(5):509–520.
14. Chang Z, Wang C. Treatment assessment of radiotherapy using MR functional quantitative imaging. World J Radiol. 2015;7(1):1. [PubMed: 25628799]
15. Le Bihan D Molecular diffusion nuclear magnetic resonance imaging. Magn Reson Q. 1991;7(1):1–30. [PubMed: 2043461]
16. Guo Y, Cai Y-Q, Cai Z-L, et al. Differentiation of clinically benign and malignant breast lesions using diffusion-weighted imaging : J Magn Res Imaging Off J Int Soc Magn Reson Med. 2002;16(2):172–178.
17. Koh D-M, Collins DJ. Diffusion-weighted MRI in the body: applications and challenges in oncology. Am J Roentgenol. 2007;188(6):1622–1635. [PubMed: 17515386]
18. Le Bihan D, Breton E, Lallemand D, Aubin M, Vignaud J, Laval-Jeantet M. Separation of diffusion and perfusion in intravoxel incoherent motion MR imaging. Radiology. 1988;168(2):497–505. [PubMed: 3393671]
19. Jones KM, Michel KA, Bankson JA, Fuller CD, Klopp AH, Venkatesan AM. Emerging magnetic resonance imaging technologies for radiation therapy planning and response assessment. Int J Radiat Oncol Biol Phys. 2018;101(5):1046–1056. [PubMed: 30012524]
20. Le Bihan D, Mangin J-F, Poupon C, et al. Diffusion tensor imaging: concepts and applications. J Magn Res Imaging Off J Int Soc Magn Res Med. 2001;13(4):534–546.
21. Basser PJ, Mattiello J, LeBihan D. Estimation of the effective self-diffusion tensor from the NMR spin echo. J Magn Reson, Ser B. 1994;103(3):247–254. [PubMed: 8019776]
22. Assaf Y, Pasternak O. Diffusion tensor imaging (DTI)-based white matter mapping in brain research: a review. J Mol Neurosci. 2008;34(1):51–61. [PubMed: 18157658]
23. Catani M, Howard RJ, Pajevic S, Jones DK. Virtual in vivo interactive dissection of white matter fasciculi in the human brain. NeuroImage. 2002;17(1):77–94. [PubMed: 12482069]
24. Basser PJ, Pajevic S, Pierpaoli C, Duda J, Aldroubi A. In vivo fiber tractography using DT-MRI data. Magn Reson Med. 2000;44(4):625–632. [PubMed: 11025519]
25. Hylton N. Dynamic contrast-enhanced magnetic resonance imaging as an imaging biomarker. J Clin Oncol. 2006;24(20):3293–3298. [PubMed: 16829653]
26. Daniel BL, Yen YF, Glover GH, et al. Breast disease: dynamic spiral MR imaging. Radiology. 1998;209(2):499–509. [PubMed: 9807580]

27. Wang C-H, Yin F-F, Horton J, Chang Z. Review of treatment assessment using DCE-MRI in breast cancer radiation therapy. World J Methodol. 2014;4(2):46. [PubMed: 25332905]
28. Tofts PS, Brix G, Buckley DL, et al. Estimating kinetic parameters from dynamic contrast-enhanced T1-weighted MRI of a diffusable tracer: standardized quantities and symbols. J Magn Reson Imaging Off J Int Soc Magn Reson Med. 1999;10(3):223–232.
29. Clare S, Jezzard P. Rapid T1 mapping using multislice echo planar imaging. Magn Reson Med Off J Int Soc Magn Reson Med. 2001;45(4):630–634.
30. Schabel MC, Morrell GR. Uncertainty in T1 mapping using the variable flip angle method with two flip angles. Phys Med Biol. 2008;54(1):N1. [PubMed: 19060359]
31. Lawrence KSS, Lee T-Y. An adiabatic approximation to the tissue homogeneity model for water exchange in the brain: I. Theoretical derivation. J Cereb Blood Flow Metab. 1998;18(12):1365–1377. [PubMed: 9850149]
32. Tofts PS, Kermode AG. Measurement of the blood-brain barrier permeability and leakage space using dynamic MR imaging. 1. Fundamental concepts. Magn Reson Med. 1991;17(2):357–367. [PubMed: 2062210]
33. Yankeelov TE, Rooney WD, Li X, Springer CS Jr. Variation of the relaxographic “shutter-speed” for transcytolemmal water exchange affects the CR bolus-tracking curve shape. Magn Res Med Off J Int Soc Magn Res Med. 2003;50(6):1151–1169.
34. Tofts PS. Modeling tracer kinetics in dynamic Gd-DTPA MR imaging. J Magn Reson Imaging. 1997;7(1):91–101. [PubMed: 9039598]
35. Port RE, Knopp MV, Hoffmann U, Milker-Zabel S, Brix G. Multicompartment analysis of gadolinium chelate kinetics: blood-tissue exchange in mammary tumors as monitored by dynamic MR imaging. J Magn Reson Imaging Off J Int Soc Magn Reson Med. 1999;10(3):233–241.
36. Wang C, Yin F-F, Kirkpatrick JP, Chang Z. Accelerated brain DCE-MRI using iterative reconstruction with total generalized variation penalty for quantitative pharmacokinetic analysis: a feasibility study. Technol Cancer Res Treat. 2017;16(4):446–460. [PubMed: 27215931]
37. Cao Y, Li D, Shen Z, Normolle D. Sensitivity of quantitative metrics derived from DCE MRI and a pharmacokinetic model to image quality and acquisition parameters. Acad Radiol. 2010;17(4):468–478. [PubMed: 20207317]
38. Khalifa F, Soliman A, El-Baz A, et al. Models and methods for analyzing DCE-MRI: a review. Med Phys. 2014;41(12):124301. [PubMed: 25471985]
39. Parker GJM, Roberts C, Macdonald A, et al. Experimentally-derived functional form for a population-averaged high-temporal-resolution arterial input function for dynamic contrast-enhanced MRI. Magn Reson Med Off J Int Soc Magn Res Med. 2006;56(5):993–1000.
40. Yankeelov TE, Luci JJ, Lepage M, et al. Quantitative pharmacokinetic analysis of DCE-MRI data without an arterial input function: a reference region model. Magn Reson Imaging. 2005;23(4):519–529. [PubMed: 15919597]
41. Shukla G, Alexander GS, Bakas S, et al. Advanced magnetic resonance imaging in glioblastoma: a review. Chin Clin Oncol. 2017;6(4):40. [PubMed: 28841802]
42. Petrella JR, Provenzale JM. MR perfusion imaging of the brain: techniques and applications. Am J Roentgenol. 2000; 175(1):207–219. [PubMed: 10882275]
43. Essig M, Shiroishi MS, Nguyen TB, et al. Perfusion MRI: the five most frequently asked technical questions. Am J Roentgenol. 2013;200(1):24–34. [PubMed: 23255738]
44. Sorensen AG, Reimer P. Cerebral MR perfusion imaging: principles and current applications. 2000.
45. Carroll TJ, Teneggi V, Jobin M, et al. Absolute quantification of cerebral blood flow with magnetic resonance, reproducibility of the method, and comparison with H215O positron emission tomography. J Cereb Blood Flow Metab. 2002;22(9):1149–1156. [PubMed: 12218421]
46. Sourbron S, Ingrisch M, Siefert A, Reiser M, Herrmann K. Quantification of cerebral blood flow, cerebral blood volume, and blood–brain-barrier leakage with DCE-MRI. Magn Reson Med Off J Int Soc Magn Res Med. 2009;62(1):205–217.
47. Stagg C, Rothman DL. Magnetic resonance spectroscopy: tools for neuroscience research and emerging clinical applications. Academic Press; 2013.

48. van der Graaf M In vivo magnetic resonance spectroscopy: basic methodology and clinical applications. Eur Biophys J. 2010;39(4):527–540. [PubMed: 19680645]
49. Kim J-H, Chang K-H, Na DG, et al. Comparison of 1.5 T and 3T 1H MR spectroscopy for human brain tumors. Korean J Radiol. 2006;7(3):156. [PubMed: 16969044]
50. Ordidge RJ, Connelly A, Lohman JA. Image-selected in vivo spectroscopy (ISIS). A new technique for spatially selective NMR spectroscopy. J Magn Reson (1969). 1986;66(2):283–294.
51. Scheenen TW, Klomp DW, Wijnen JP, Heerschap A. Short echo time 1H-MRSI of the human brain at 3T with minimal chemical shift displacement errors using adiabatic refocusing pulses. Magn Res Med Off J Int Soc Magn Reson Med. 2008;59(1):1–6.
52. Haase A, Frahm J, Hanicke W, Matthaei D. 1H NMR chemical shift selective (CHESS) imaging. Phys Med Biol. 1985;30(4):341. [PubMed: 4001160]
53. Maudsley AA, Matson G, Hugg J, Weiner M. Reduced phase encoding in spectroscopic imaging. Magn Reson Med. 1994;31(6):645–651. [PubMed: 8057817]
54. Weinreb JC, Barentsz JO, Choyke PL, et al. PI-RADS prostate imaging–reporting and data system: 2015, version 2. Eur Urol. 2016;69(1):16–40. [PubMed: 26427566]
55. Pinker K, Stadlbauer A, Bogner W, Gruber S, Helbich T. Molecular imaging of cancer: MR spectroscopy and beyond. Eur J Radiol: 2012;81(3):566–577. [PubMed: 20554145]
56. Herris AL. Hypoxia—a key regulatory factor in tumour growth. Nat Rev Cancer. 2002;2(1):38–47. [PubMed: 11902584]
57. Overgaard J. Hypoxic radiosensitization: adored and ignored. J Clin Oncol. 2007;25(26):4066–4074. [PubMed: 17827455]
58. Howe F, Robinson S, McIntyre D, Stubbs M, Griffiths J. Issues in flow and oxygenation dependent contrast (FLOOD) imaging of tumours. NMR Biomed Int J Devot Dev Appl Magnet Reson Vivo. 2001;14(7–8):497–506.
59. O'Connor JPB, Jackson A, Buonaccorsi GA, et al. Organ-specific effects of oxygen and carbogen gas inhalation on tissue longitudinal relaxation times. Magn Reson Med Off J Int Soc Magn Reson Med. 2007;58(3):490–496.
60. Gray LH, Conger AD, Ebert M, Hornsey S, Scott O. The concentration of oxygen dissolved in tissues at the time of irradiation as a factor in radiotherapy. Br J Radiol. 1953;26(312):638–648. [PubMed: 13106296]
61. Hallac RR, Zhou H, Pidikiti R, et al. Correlations of noninvasive BOLD and TOLD MRI with pO2 and relevance to tumor radiation response. Magn Reson Med. 2014;71(5):1863–1873. [PubMed: 23813468]
62. Margaret Cheng HL, Stikov N, Ghugre NR, Wright GA. Practical medical applications of quantitative MR relaxometry. J Magn Reson Imaging. 2012;36(4):805–824. [PubMed: 22987758]
63. Ma D, Gulani V, Seiberlich N, et al. Magnetic resonance fingerprinting. Nature. 2013;495(7440):187–192. [PubMed: 23486058]
64. Panda A, Mehta BB, Coppo S, et al. Magnetic resonance finger-printing–an overview. Curr Opin Biomed Eng. 2017;3:56–66. [PubMed: 29868647]
65. Lemasson B, Pannetier N, Coquery N, et al. MR vascular fingerprinting in stroke and brain tumors models. Sci Rep. 2016;6(1):1–11. [PubMed: 28442746]
66. Su P, Mao D, Liu P, et al. Multiparametric estimation of brain hemodynamics with MR fingerprinting ASL. Magn Reson Med. 2017;78(5):1812–1823. [PubMed: 28019021]
67. Jones KM, Pollard AC, Pagel MD. Clinical applications of chemical exchange saturation transfer (CEST) MRI. J Magn Reson Imaging. 2018;47(1):11–27. [PubMed: 28792646]
68. Wu B, Warnock G, Zaiss M, et al. An overview of CEST MRI for non-MR physicists. EJNMMI physics. 2016;3(1):1–21. [PubMed: 26782039]
69. Harston GWJ, Tee YK, Blockley N, et al. Identifying the ischaemic penumbra using pH-weighted magnetic resonance imaging. Brain. 2015;138(1):36–42. [PubMed: 25564491]
70. Matzat SJ, van Tiel J, Gold GE, Oei EH. Quantitative MRI techniques of cartilage composition. Quant Imaging Med Surg. 2013;3(3):162. [PubMed: 23833729]
71. Wang L, Chang G, Xu J, et al. T1rho MRI of menisci and cartilage in patients with osteoarthritis at 3T. Eur J Radiol. 2012;81(9):2329–2336. [PubMed: 21908122]

72. Stahl R, Luke A, Li X, et al. T1rho, T 2 and focal knee cartilage abnormalities in physically active and sedentary healthy subjects versus early OA patients—A 3.0-tesla MRI study. Eus Radiol. 2009;19(1):132–143.
73. Gallagher FA, Kettunen MI, Hu D-E, et al. Production of hyperpolarized [1, 4–13C2] malate from [1, 4–13C2] fumarate is a marker of cell necrosis and treatment response in tumors. Proc Natl Acad Sci. 2009;106(47):19801–19806. [PubMed: 19903889]
74. Wilson DM, Keshari KR, Larson PEZ, et al. Multi-compound polarization by DNP allows simultaneous assessment of multiple enzymatic activities in vivo. J Magn Reson. 2010;205(1):141–147. [PubMed: 20478721]
75. Vander Heiden MG, Cantley LC, Thompson CB. Understanding the Warburg effect: the metabolic requirements of cell proliferation. Science. 2009;324(5930):1029–1033. [PubMed: 19460998]
76. Aerts HJWL, Velazquez ER, Leijenaar RTH, et al. Decoding tumour phenotype by noninvasive imaging using a quantitative radiomics approach. Nat Commun. 2014;5(1):1–9.
77. Yip SS, Aerts HJ. Applications and limitations of radiomics. Phys Med Biol. 2016;61(13):R150. [PubMed: 27269645]
78. Gillies RJ, Kinahan PE, Hricak H. Radiomics: images are more than pictures, they are data. Radiology. 2016;278(2):563–577. [PubMed: 26579733]
79. Louis DN, Perry A, Reifenberger G, et al. The 2016 World Health Organization classification of tumors of the central nervous system: a summary. Acta Neuropathol. 2016;131(6):803–820. [PubMed: 27157931]
80. Ostrom QT, Cioffi G, Gittleman H , et al. CBTRUS statistical report: primary brain and other central nervous system tumors diagnosed in the United States in 2012–2016. Neuro-oncology. 2019;21(Supplement_5):v1–v100. [PubMed: 31675094]
81. Stupp R, Mason WP, van den Bent MJ, et al. Radiotherapy plus concomitant and adjuvant temozolomide for glioblastoma. N Engl J Med. 2005;352(10):987–996. [PubMed: 15758009]
82. Bell EH, Pugh SL, McElroy JP, et al. Molecular-based recursive partitioning analysis model for glioblastoma in the temozolomide era: a correlative analysis based on NRG oncology RTOG 0525. JAMA Oncology. 2017;3(6):784–792. [PubMed: 28097324]
83. Stupp R, Taillibert S, Kanner A, et al. Effect of tumor-treating fields plus maintenance temozolomide vs maintenance temozolomide alone on survival in patients with glioblastoma: a randomized clinical trial. JAMA. 2017;318(23):2306–2316. [PubMed: 29260225]
84. van Dijken BR, van Laar PJ, Holtman GA, van der Hoorn A. Diagnostic accuracy of magnetic resonance imaging techniques for treatment response evaluation in patients with high-grade glioma, a systematic review and meta-analysis. Eur Radiol. 2017;27(10):4129–4144. [PubMed: 28332014]
85. Wen PY, Macdonald DR, Reardon DA, et al. Updated response assessment criteria for high-grade gliomas: response assessment in neuro-oncology working group. J Clin Oncol. 2010;28(11):1963–1972. [PubMed: 20231676]
86. Cordova JS. Shu H-K, Liang Z, et al. Whole-brain spectroscopic MRI biomarkers identify infiltrating margins in glioblastoma patients. Neuro-oncology. 2016;18(8):1180–1189. [PubMed: 26984746]
87. Taal W, Brandsma D, de Bruin HG, et al. Incidence of early pseudo-progression in a cohort of malignant glioma patients treated with chemoirradiation with temozolomide. Cancer. 2008;113(2):405–410. [PubMed: 18484594]
88. Brandes AA, Franceschi E, Tosoni A. et al. MGMT promoter methylation status can predict the incidence and outcome of pseudoprogression after concomitant radiochemotherapy in newly diagnosed glioblastoma patients. J Clin Oncol. 2008;26(13):2192–2197. [PubMed: 18445844]
89. Stewart J, Sahgal A, Lee Y, et al. Quantitating interfraction target dynamics during concurrent chemoradiation for glioblastoma: a prospective serial imaging study. Int J Radiat Oncol Biol Phys. 2020;109(3):736–746. [PubMed: 33068687]
90. Fabi A, Russillo M, Metro G, Vidiri A, Di Giovanni S, Cognetti F. Pseudoprogression and MGMT status in glioblastoma patients: implications in clinical practice. Anticancer Res. 2009;29(7):2607–2610. [PubMed: 19596935]

91. Chaskis C, Neyns B, Michotte A, De Ridder M, Everaert H. Pseudoprogression after radiotherapy with concurrent temozolomide for high-grade glioma: clinical observations and working recommendations. Surg Neurol. 2009;72(4):423–428. [PubMed: 19150114]
92. Brandes AA, Tosoni A, Spagnolli F, et al. Disease progression or pseudoprogression after concomitant radiochemotherapy treatment: pitfalls in neurooncology. Neuro-oncology. 2008;10(3):361–367. [PubMed: 18401015]
93. Kargiotis O, Geka A, Rao JS, Kyritsis AP. Effects of irradiation on tumor cell survival, invasion and angiogenesis. J Neurooncol. 2010;100(3):323–338. [PubMed: 20449629]
94. Giglio P, Gilbert MR. Cerebral radiation necrosis. The neurologist. 2003;9(4):180–188. [PubMed: 12864928]
95. Ellingson BM, Malkin MG, Rand SD, et al. Validation of functional diffusion maps (fDMs) as a biomarker for human glioma cellularity. J Magn Reson Imaging Off J Int Soc Magnet Res Med. 2010;31(3):538–548.
96. Nakamura H, Murakami R, Hirai T, Kitajima M, Yamashita Y. Can MRI-derived factors predict the survival in glioblastoma patients treated with postoperative chemoradiation therapy? Acta Radiol. 2013;54(2):214–220. [PubMed: 23138021]
97. Hamstra DA, Galbán CJ, Meyer CR et al. Functional diffusion map as an early imaging biomarker for high-grade glioma: correlation with conventional radiologic response and overall survival. J Clin Oncol. 2008;26(20):3387. [PubMed: 18541899]
98. Wang S, Martinez-Lage M, Sakai Y, et al. Differentiating tumor progression from pseudoprogression in patients with glioblastomas using diffusion tensor imaging and dynamic susceptibility contrast MRI. Am J Neuroradiol 2016;37(1):28–36. [PubMed: 26450533]
99. Elson A, Bovi J, Siker M, Schultz C, Paulson E. Evaluation of absolute and normalized apparent diffusion coefficient (ADC) values within the post-operative T2/FLAIR volume as adverse prognostic indicators in glioblastoma. J Neurooncol. 2015;122(3):549–558. [PubMed: 25700835]
100. Barajas RF, Chang JS, Segal MR, et al. Differentiation of recurrent glioblastoma multiforme from radiation necrosis after external beam radiation therapy with dynamic susceptibility-weighted contrast-enhanced perfusion MR imaging. Radiology. 2009;253(2):486–496. [PubMed: 19789240]
101. Hu LS, Baxter LC, Smith KA, et al. Relative cerebral blood volume values to differentiate high-grade glioma recurrence from posttreatment radiation effect: direct correlation between image-guided tissue histopathology and localized dynamic susceptibility-weighted contrast-enhanced perfusion MR imaging measurements. Am J Neuroradiol. 2009;30(3):552–558. [PubMed: 19056837]
102. Mangla R, Singh G, Ziegelitz D, et al. Changes in relative cerebral blood volume 1 month after radiation-temozolomide therapy can help predict overall survival in patients with glioblastoma. Radiology. 2010;256(2):575–584. [PubMed: 20529987]
103. Larsson C, Groote I, Vardal J, et al. Prediction of survival and progression in glioblastoma patients using temporal perfusion changes during radiochemotherapy. Magn Reson Imaging. 2020;68:106–112. [PubMed: 32004711]
104. Choi YJ, Kim HS, Jahng G-H, Kim SJ, Suh DC. Pseudoprogression in patients with glioblastoma: added value of arterial spin labeling to dynamic susceptibility contrast perfusion MR imaging. Acta Radiol. 2013;54(4):448–454. [PubMed: 23592805]
105. Xu Q, Liu QI, Ge H, et al. Tumor recurrence versus treatment effects in glioma: a comparative study of three dimensional pseudo-continuous arterial spin labeling and dynamic susceptibility contrast imaging. Medicine. 2017;96(50).
106. Federau C, Cerny M, Roux M, et al. IVIM perfusion fraction is prognostic for survival in brain glioma. Clinical Neuroradiol. 2017;27(4):485–492.
107. Di Costanzo A, Trojsi F, Giannatempo G, et al. Spectroscopic, diffusion and perfusion magnetic resonance imaging at 3.0 Tesla in the delineation of glioblastomas: preliminary results. J Exp Clin Cancer Res. 2006;25(3):385.
108. Pirzkall A, McKnight TR, Graves EE, et al. MR-spectroscopy guided target delineation for high-grade gliomas. Int J Radiat Oncol Biol Phys. 2001;50(4):915–928. [PubMed: 11429219]

109. Quon H, Brunet B, Alexander A, et al. Changes in serial magnetic resonance spectroscopy predict outcome in high-grade glioma during and after postoperative radiotherapy. Anticancer Res. 2011;31(10):3559–3565. [PubMed: 21965778]
110. Muruganandham M, Clerkin PP, Smith BJ, et al. 3-Dimensional magnetic resonance spectroscopic imaging at 3 Tesla for early response assessment of glioblastoma patients during external beam radiation therapy. Int J Radiat Oncol Biol Phys. 2014;90(1):181–189. [PubMed: 24986746]
111. Chan RW, Chen H, Myrehaug S, et al. Quantitative CEST and MT at 1.5 T for monitoring treatment response in glioblastoma: early and late tumor progression during chemoradiation. J Neurooncol. 2021;151(2):267–278. [PubMed: 33196965]
112. Hein PA, Eskey CJ, Dunn JF, Hug EB. Diffusion-weighted imaging in the follow-up of treated high-grade gliomas: tumor recurrence versus radiation injury. Am J Neuroradiol. 2004;25(2):201–209. [PubMed: 14970018]
113. Chang PD, Chow DS, Yang PH, Filippi CG, Lignelli A. Predicting glioblastoma recurrence by early changes in the apparent diffusion coefficient value and signal intensity on FLAIR images. Am J Roentgenol. 2017;208(1):57–65. [PubMed: 27726412]
114. Asao C, Korogi Y, Kitajima M, et al. Diffusion-weighted imaging of radiation-induced brain injury for differentiation from tumor recurrence. Am J Neuroradiol. 2005;26(6):1455–1460. [PubMed: 15956515]
115. Thomas AA, Arevalo-Perez J, Kaley T, et al. Dynamic contrast enhanced T1 MRI perfusion differentiates pseudoprogression from recurrent glioblastoma. J Neurooncol. 2015;125(1):183–190. [PubMed: 26275367]
116. Bisdas S, Naegele T, Ritz R, et al. Distinguishing recurrent high-grade gliomas from radiation injury: a pilot study using dynamic contrast-enhanced MR imaging. Acad Radiol. 2011;18(5):575–583. [PubMed: 21419671]
117. Ozsunar Y, Mullins ME, Kwong K, et al. Glioma recurrence versus radiation necrosis?: a pilot comparison of arterial spin-labeled, dynamic susceptibility contrast enhanced MRI, and FDG-PET imaging. Acad Radiol. 2010;17(3):282–290. [PubMed: 20060750]
118. Anbarloui MR, Ghodsi SM, Khoshnevisan A, et al. Accuracy of magnetic resonance spectroscopy in distinction between radiation necrosis and recurrence of brain tumors. Iranian J Neurol. 2015;14(1):29.
119. Howe FA, Barton SJ, Cudlip SA, et al. Metabolic profiles of human brain tumors using quantitative in vivo 1H magnetic resonance spectroscopy. Magnet Reson Med Off J Int Soc Magn Reson Med. 2003;49(2):223–232.
120. Chernov MF, Hayashi M, Izawa M, et al. Multivoxel proton MRS for differentiation of radiation-induced necrosis and tumor recurrence after gamma knife radiosurgery for brain metastases. Brain Tumor Pathol. 2006;23(1):19–27. [PubMed: 18095115]
121. Nael K Bauer AH, Hormigo A, et al. Multiparametric MRI for differentiation of radiation necrosis from recurrent tumor in patients with treated glioblastoma. Am J Roentgenol. 2018;210(1):18–23. [PubMed: 28952810]
122. Cha J, Kim ST, Kim H-J, et al. Differentiation of tumor progression from pseudoprogression in patients with posttreatment glioblastoma using multiparametric histogram analysis. Am J Neuroradiol. 2014;35(7):1309–1317. [PubMed: 24676005]
123. Seeger A, Braun C, Skardelly M, et al. Comparison of three different MR perfusion techniques and MR spectroscopy for multiparametric assessment in distinguishing recurrent high-grade gliomas from stable disease. Acad Radiol. 2013;20(12):1557–1565. [PubMed: 24200483]
124. Di Costanzo A, Scarabino T, Trojsi F, et al. Recurrent glioblastoma multiforme versus radiation injury: a multiparametric 3-T MR approach. Radiol Med (Torino). 2014;119(8):616–624. [PubMed: 24408041]
125. Kim JY, Park JE, Jo Y, et al. Incorporating diffusion-and perfusion-weighted MRI into a radiomics model improves diagnostic performance for pseudoprogression in glioblastoma patients. Neuro-oncology. 2019;21(3):404–414. [PubMed: 30107606]

126. Hu X, Wong KK, Young GS, Guo L, Wong ST. Support vector machine multiparametric MRI identification of pseudoprogression from tumor recurrence in patients with resected glioblastoma. J Magn Reson Imaging. 2011;33(2):296–305. [PubMed: 21274970]

127. Lee J, Wang N, Turk S, et al. Discriminating pseudoprogression and true progression in diffuse infiltrating glioma using multi-parametric MRI data through deep learning. Sci Rep. 2020;10(1):1–10. [PubMed: 31913322]

128. Wu L-M, Hu J-N, Gu H-Y, Hua J, Chen J, Xu J-R. Can diffusion-weighted MR imaging and contrast-enhanced MR imaging precisely evaluate and predict pathological response to neoadjuvant chemotherapy in patients with breast cancer? Breast Cancer Res Treat. 2012;135(1):17–28. [PubMed: 22476850]

129. Ring A, Webb A, Ashley S, et al. Is surgery necessary after complete clinical remission following neoadjuvant chemotherapy for early breast cancer? J Clin Oncol. 2003;21(24):4540–4545. [PubMed: 14673041]

130. Chen JH, Feig B, Agrawal G, et al. MRI evaluation of pathologically complete response and residual tumors in breast cancer after neoadjuvant chemotherapy. Cancer: Interdisciplinary International Journal of the American Cancer. Society. 2008;112(1):17–26.

131. De Los Santos JF, Cantor A, Amos KD, et al. Magnetic resonance imaging as a predictor of pathologic response in patients treated with neoadjuvant systemic treatment for operable breast cancer: Translational Breast Cancer Research Consortium trial 017. Cancer. 2013;119(10):1776–1783. [PubMed: 23436342]

132. Hayashi Y, Takei H, Nozu S, et al. Analysis of complete response by MRI following neoadjuvant chemotherapy predicts pathological tumor responses differently for molecular subtypes of breast cancer Corrigendum in/ol/5/4/1433. Oncol Lett. 2013;5(1):83–89. [PubMed: 23255899]

133. Garcia-Tejedor A, Fernandez-Gonzalez S, Ortega R, et al. Can we avoid axillary lymph node dissection in N2 breast cancer patients with chemo-sensitive tumours such as HER2 and TNBC? Breast Cancer Res Treat. 2020;185(3):657–666. [PubMed: 33068198]

134. Bazan JG, White J. Imaging of the axilla before preoperative chemotherapy: implications for postmastectomy radiation. Cancer. 2015;121(8):1187–1194. [PubMed: 25288389]

135. Paudel N, Bethke KP, Wang LC, Strauss JB, Hayes JP, Donnelly ED. Impact of breast MRI in women eligible for breast conservation surgery and intra-operative radiation therapy. Surg Oncol. 2018;27(1):95–99. [PubMed: 29549911]

136. Krengli M, Pisani C, Deantonio L. Patient selection for partial breast irradiation by intraoperative radiation therapy: can magnetic resonance imaging be useful?—perspective from radiation oncology point of view. J Thorac Dis. 2016;8(9):E987. [PubMed: 27747042]

137. Tallet A, Rua S, Jalaguier A, et al. Impact of preoperative magnetic resonance imaging in breast cancer patients candidates for an intraoperative partial breast irradiation. Hong Kong: AME Publishing Company. 2015;183.

138. Wang C, Horton JK, Yin F-F, Chang Z. Assessment of treatment response with diffusion-weighted MRI and dynamic contrast-enhanced MRI in patients with early-stage breast cancer treated with single-dose preoperative radiotherapy: initial results. Technol Cancer Res Treat. 2016;15(5):651–660. [PubMed: 26134438]

139. Mouawad M, Biernaski H, Brackstone M, et al. DCE-MRI assessment of response to neoadjuvant SABR in early stage breast cancer: comparisons of single versus three fraction schemes and two different imaging time delays post-SABR. Clini Translat Radiat Oncol. 2020;21:25–31.

140. Charaghvandi RK, van Asselen B, Philippens MEP, et al. Redefining radiotherapy for early-stage breast cancer with single dose ablative treatment: a study protocol. BMC Cancer. 2017;17(1):1–9. [PubMed: 28049525]

141. Vasmel JE, Charaghvandi RK, Houweling AC, et al. Tumor response after neoadjuvant magnetic resonance guided single ablative dose partial breast irradiation. Int J Radiat Oncol Biol Phys. 2020;106(4):821–829. [PubMed: 31812720]

142. Tahmassebi A, Wengert GJ, Helbich TH, et al. Impact of machine learning with multiparametric magnetic resonance imaging of the breast for early prediction of response to neoadjuvant chemotherapy and survival outcomes in breast cancer patients. Invest Radiol. 2019;54(2):110–117. [PubMed: 30358693]

143. Liu Z, Li Z, Qu J, et al. Radiomics of multiparametric MRI for pretreatment prediction of pathologic complete response to neoadjuvant chemotherapy in breast cancer: a multicenter study. Clin Cancer Res. 2019;25(12):3538–3547. [PubMed: 30842125]

144. Fütterer JJ, Briganti A, De Visschere P, et al. Can clinically significant prostate cancer be detected with multiparametric magnetic resonance imaging? A systematic review of the literature. Eur Urol. 2015;68(6):1045–1053. [PubMed: 25656808]

145. Morris WJ, Tyldesle S, Rodda S, et al. Androgen Suppression Combined with Elective Nodal and Dose Escalated Radiation Therapy (the ASCENDE-RT Trial): an analysis of survival endpoints for a randomized trial comparing a low-dose-rate brachytherapy boost to a dose-escalated external beam boost for high-and intermediate-risk prostate cancer. Int J Radiat Oncol Biol Phys. 2017;98(2):275–285. [PubMed: 28262473]

146. Stoyanova R, Chinea F, Kwon D, et al. An automated multiparametric MRI quantitative imaging prostate habitat risk scoring system for defining external beam radiation therapy boost volumes. Int J Radiat Oncol Biol Phys. 2018;102(4):821–829. [PubMed: 29908220]

147. Lips IM, van der Heide UA, Haustermans K, et al. Single blind randomized phase III trial to investigate the benefit of a focal lesion ablative microboost in prostate cancer (FLAME-trial): study protocol for a randomized controlled trial. Trials. 2011;12(1):1–11. [PubMed: 21199584]

148. Pollack A, Chinea FM, Bossart E et al. , Phase I trial of MRI-guided prostate cancer lattice extreme ablative dose (LEAD) boost radiation therapy. Int J Radiat Oncol Biol Phys. 2020;107(2):305–315. [PubMed: 32084522]

149. Barrett T, Gill AB, Kataoka MY, et al. DCE and DW MRI in monitoring response to androgen deprivation therapy in patients with prostate cancer: a feasibility study. Magn Reson Med. 2012;67(3):778–785. [PubMed: 22135228]

150. Song I, Kim CK, Park BK, Park W. Assessment of response to radiotherapy for prostate cancer: value of diffusion-weighted MRI at 3 T. Am J Roentgenol. 2010;194(6):W477–W482. [PubMed: 20489065]

151. Wu X, Reinikainen P, Kapanen M, et al. Monitoring radiotherapy induced tissue changes in localized prostate cancer by multi-parametric magnetic resonance imaging (MP-MRI). Diagn Int Imaging. 2019;100(11):699–708.

152. Akin O, Gultekin DH, Vargas HA, et al. Incremental value of diffusion weighted and dynamic contrast enhanced MRI in the detection of locally recurrent prostate cancer after radiation treatment: preliminary results. Eur Radiol. 2011;21(9):1970–1978. [PubMed: 21533634]

153. Foltz WD, Wu A, Chung P, et al. Changes in apparent diffusion coefficient and T2 relaxation during radiotherapy for prostate cancer. J Magn Reson Imaging. 2013;37(4):909–916. [PubMed: 23097411]

154. van Schie MA, van Houdt PJ, Ghobadi G, et al. Quantitative MRI changes during weekly ultra-hypofractionated prostate cancer radiotherapy with integrated boost. Front Oncol. 2019;9:1264. [PubMed: 31867266]

155. Franiel T, Lüdemann L, Taupitz M, Böhmer D, Beyersdorff D. MRI before and after external beam intensity-modulated radiotherapy of patients with prostate cancer: the feasibility of monitoring of radiation-induced tissue changes using a dynamic contrast-enhanced inversion-prepared dual-contrast gradient echo sequence. Radiother Oncol. 2009;93(2):241–245. [PubMed: 19748143]

156. Delgadillo R, Ford JC, Abramowitz MC, Dal Pra A, Pollack A, Stoyanova R. The role of radiomics in prostate cancer radiotherapy. Strahlenther Onkol. 2020;196(10):900–912. [PubMed: 32821953]

157. Abdollahi H, Mofid B, Shiri I, et al. Machine learning-based radiomic models to predict intensity-modulated radiation therapy response, Gleason score and stage in prostate cancer. Radiol Med (Torino). 2019;124(6):555–567. [PubMed: 30607868]

158. Siegel RL, Miller KD, Jemal A, Cancer statistics 2016. CA: Cancer J Clin. 2016;66(1):7–30. [PubMed: 26742998]

159. Jansen JF, Parra C, Lu Y, Shukla-Dave A. Evaluation of head and neck tumors with functional MR imaging. Magn Reson Imaging Clin. 2016;24(1):123–133.

160. Vokes EE, Weichselbaum RR, Lippman SM, Hong WK. Head and neck cancer. N Engl J Med. 1993;328(3):184–194. [PubMed: 8417385]

161. Pignon JP, Bourhis J, Domenge C, Designé L, Group M-NC. Chemotherapy added to locoregional treatment for head and neck squamous-cell carcinoma: three meta-analyses of updated individual data. Lancet. 2000;355(9208):949–955. [PubMed: 10768432]

162. Wang X, Eisbruch A. IMRT for head and neck cancer: reducing xerostomia and dysphagia. J Radiat Res. 2016;57(S1):i69–i75. [PubMed: 27538846]

163. Eisbruch A, Harris J, Garden AS, et al. Multi-institutional trial of accelerated hypofractionated intensity-modulated radiation therapy for early-stage oropharyngeal cancer (RTOG 00–22). Int J Radiat Oncol Biol Phys. 2010;76(5):1333–1338. [PubMed: 19540060]

164. Eisbruch A, Dawson L, Kim H, et al. Conformal and intensity modulated irradiation of head and neck cancer: the potential for improved target irradiation, salivary gland function, and quality of life. Acta Otorhinolaryngol Belg. 1999;53(3):271–275. [PubMed: 10635407]

165. Kam MKM, Leung S-F, Zee B, et al. Prospective randomized study of intensity-modulated radiotherapy on salivary gland function in early-stage nasopharyngeal carcinoma patients. J Clin Oncol. 2007;25(31):4873–4879. [PubMed: 17971582]

166. Kim S, Loevner L, Quon H, et al. Diffusion-weighted magnetic resonance imaging for predicting and detecting early response to chemoradiation therapy of squamous cell carcinomas of the head and neck. Clin Cancer Res. 2009;15(3):986–994. [PubMed: 19188170]

167. Dirix P, De Keyzer F, Vandecaveye V, Stroobants S, Hermans R, Nuyts S. Diffusion-weighted magnetic resonance imaging to evaluate major salivary gland function before and after radiotherapy. Int J Radiat Oncol Biol Phys. 2008;71(5):1365–1371. [PubMed: 18355977]

168. Scalco E, Marzi S, Sanguineti G, Vidiri A, Rizzo G. Characterization of cervical lymph-nodes using a multi-parametric and multi-modal approach for an early prediction of tumor response to chemo-radiotherapy. Physica Med. 2016;32(12):1672–1680.

169. Dirix P, Vandecaveye V, De Keyzer F, Stroobants S, Hermans R, Nuyts S. Dose painting in radiotherapy for head and neck squamous cell carcinoma: value of repeated functional imaging with 18F-FDG PET, 18F-fluoromisonidazole PET, diffusion-weighted MRI, and dynamic contrast-enhanced MRI. J Nucl Med. 2009;50(7):1020–1027. [PubMed: 19525447]

170. Ng S-H, Liao C-T, Lin C-Y, et al. Dynamic contrast-enhanced MRI, diffusion-weighted MRI and 18 F-FDG PET/CT for the prediction of survival in oropharyngeal or hypopharyngeal squamous cell carcinoma treated with chemoradiation. Eur Radiol. 2016;26(11):4162–4172. [PubMed: 26911889]

171. Jansen JFA, Schöder H, Lee NY, et al. Tumor metabolism and perfusion in head and neck squamous cell carcinoma: pre-treatment multimodality imaging with 1H magnetic resonance spectroscopy, dynamic contrast-enhanced MRI, and [18F] FDG-PET. Int J Radiat Oncol Biol Phys. 2012;82(1):299–307. [PubMed: 21236594]

172. Zhou N, Chu C, Dou X, et al. Early changes of irradiated parotid glands evaluated by T1rho-weighted imaging: a pilot study. J Comput Assist Tomogr. 2017;41(3):472–476. [PubMed: 27824671]

173. Pham TT, Liney GP, Wong K, Barton MB. Functional MRI for quantitative treatment response prediction in locally advanced rectal cancer. Br J Radiol. 2017;90(1072):20151078. [PubMed: 28055248]

174. Blazic IM, Campbell NM, Gollub MJ. MRI for evaluation of treatment response in rectal cancer. Br J Radiol. 2016;89(1064):20150964. [PubMed: 27331883]

175. Attenberger UI, Ong MM, Rathmann N, et al. mMRI at 3.0 T as an evaluation tool of therapeutic response to neoadjuvant CRT in patients with advanced-stage rectal cancer. Anticancer Res. 2017;37(1):215–222. [PubMed: 28011494]

176. Dzik-Jurasz A, Domenig C, George M, et al. Diffusion MRI for prediction of response of rectal cancer to chemoradiation. The Lancet. 2002;360(9329):307–308.

177. Genovesi D, Filippone A, Ausili Cèfaro G, et al. Diffusion-weighted magnetic resonance for prediction of response after neoadjuvant chemoradiation therapy for locally advanced rectal cancer: preliminary results of a monoinstitutional prospective study. Eur J Surg Oncol (EJSO). 2013;39(10):1071–1078. [PubMed: 23953231]

178. Jang K, Kim S, Choi D, Lee S, Park M, Min K. Pathological correlation with diffusion restriction on diffusion-weighted imaging in patients with pathological complete response after neoadjuvant chemoradiation therapy for locally advanced rectal cancer: preliminary results. Br J Radiol. 2012;85(1017):e566–e572. [PubMed: 22422387]

179. Sun Y-S, Zhang X-P, Tang L, et al. Locally advanced rectal carcinoma treated with preoperative chemotherapy and radiation therapy: preliminary analysis of diffusion-weighted MR imaging for early detection of tumor histopathologic downstaging. Radiology. 2010;254(1):170–178. [PubMed: 20019139]

180. Curvo-Semedo L, Lambregts DMJ, Maas M, et al. Rectal cancer: assessment of complete response to preoperative combined radiation therapy with chemotherapy—conventional MR volumetry versus diffusion-weighted MR imaging. Radiology. 2011;260(3):734–743. [PubMed: 21673229]

181. Lambregts DMJ, Maas M, Riedl RG, et al. Value of ADC measurements for nodal staging after chemoradiation in locally advanced rectal cancer—a per lesion validation study. Eur Radiol. 2011;21(2):265–273. [PubMed: 20730540]

182. Maas M, Lambregts DMJ, Nelemans PJ, et al. Assessment of clinical complete response after chemoradiation for rectal cancer with digital rectal examination, endoscopy, and MRI: selection for organ-saving treatment. Ann Surg Oncol. 2015;22(12):3873–3880. [PubMed: 26198074]

183. Kim SH, Lee JM, Hong SH, et al. Locally advanced rectal cancer: added value of diffusion-weighted MR imaging in the evaluation of tumor response to neoadjuvant chemo-and radiation therapy. Radiology. 2009;253(1):116–125. [PubMed: 19789256]

184. de Lussanet QG, Backes WH, Griffioen AW, et al. ; Dynamic contrast-enhanced magnetic resonance imaging of radiation therapy-induced microcirculation changes in rectal cancer. Int J Radiat Oncol Biol Phys. 2005;63(5):1309–1315. [PubMed: 16125874]

185. Intven M, Monninkhof EM, Reerink O, Philippens ME. Combined T2w volumetry, DW-MRI and DCE-MRI for response assessment after neo-adjuvant chemoradiation in locally advanced rectal cancer. Acta Oncol. 2015;54(10):1729–1736. [PubMed: 25914930]

186. Intven M, Reerink O, Philippens ME. Dynamic contrast enhanced MR imaging for rectal cancer response assessment after neo-adjuvant chemoradiation. J Magn Reson Imaging. 2015;41(6):1646–1653. [PubMed: 25124320]

187. Kim SH, Lee JM, Gupta SN, Han JK, Choi BI. Dynamic contrast-enhanced MRI to evaluate the therapeutic response to neoadjuvant chemoradiation therapy in locally advanced rectal cancer. J Magn Reson Imaging. 2014;40(3):730–737. [PubMed: 24307571]

188. Tong T, Sun Y, Gollub MJ, et al. Dynamic contrast-enhanced MRI: Use in predicting pathological complete response to neoadjuvant chemoradiation in locally advanced rectal cancer. J Magn Reson Imaging. 2015;42(3):673–680. [PubMed: 25652254]

189. Cerny M, Dunet V, Rebecchini C, et al. Response of locally advanced rectal cancer (LARC) to radiochemotherapy: DW-MRI and multiparametric PET/CT in correlation with histopathology. Nuklearmedizin. 2019;58(01):28–38. [PubMed: 30769371]

190. Hötker AM, Tarlinton L, Mazaheri Y, et al. Multiparametric MRI in the assessment of response of rectal cancer to neoadjuvant chemoradiotherapy: A comparison of morphological, volumetric and functional MRI parameters. Eur Radiol. 2016;26(12):4303–4312. [PubMed: 26945761]

191. Kremser C, Trieb T, Rudisch A, Judmaier W, de Vries A. Dynamic T1 mapping predicts outcome of chemoradiation therapy in primary rectal carcinoma: sequence implementation and data analysis. J Magnet Reson Imaging Off J Int Soc Magn Res Med. 2007;26(3):662–671.

192. Hötker AM, Garcia-Aguilar J, Gollub MJ. Multiparametric MRI of rectal cancer in the assessment of response to therapy: a systematic review. Dis Colon Rectum. 2014;57(6):790–799. [PubMed: 24807605]

193. Fusco R, Sansone M, Granata V, et al. Diffusion and perfusion MR parameters to assess preoperative short-course radiotherapy response in locally advanced rectal cancer: a comparative explorative study among Standardized Index of Shape by DCE-MRI, intravoxel incoherent motion-and diffusion kurtosis imaging-derived parameters. Abdom Radiol. 2019;44(11):3683–3700.

194. Schurink NW, Min LA, Berbee M, et al. Value of combined multiparametric MRI and FDG-PET/CT to identify well-responding rectal cancer patients before the start of neoadjuvant chemoradiation. Eur Radiol. 2020;30(5):2945–2954. [PubMed: 32034488]

195. Song I,Kim SH, Lee S, Choi J, Kim MJ, Rhim H. Value of diffusion-weighted imaging in the detection of viable tumour after neoadjuvant chemoradiation therapy in patients with locally advanced rectal cancer: comparison with T 2 weighted and PET/CT imaging. Br J Radiol. 2012;85(1013):577–586. [PubMed: 21343320]

196. network GEg. EMBRACE. https://www.embracestudy.dk/Public/Default.aspx?ReturnUrl=%2f&AspxAutoDetectCookieSupport=1

197. Daniel M, Andrzejewski P, Sturdza A, et al. Impact of hybrid PET/MR technology on multiparametric imaging and treatment response assessment of cervix cancer. Radiother Oncol. 2017;125(3):420–425. [PubMed: 29153465]

198. Georg P, Andrzejewski P, Baltzer P, et al. Changes in tumor biology during chemoradiation of cervix cancer assessed by multiparametric MRI and hypoxia PET. Mol Imag Biol. 2018;20(1):160–169.

199. Onal C, Erbay G, Guler OC. Treatment response evaluation using the mean apparent diffusion coefficient in cervical cancer patients treated with definitive chemoradiotherapy. J Magn Reson Imaging. 2016;44(4):1010–1019. [PubMed: 26919800]

200. Sarabhai T, Tschischka A, Stebner V, et al. Simultaneous multiparametric PET/MRI for the assessment of therapeutic response to chemotherapy or concurrent chemoradiotherapy of cervical cancer patients: preliminary results. Clin Imaging. 2018;49:163–168. [PubMed: 29554613]

201. Yang W, Qiang JW, Tian HP, Chen B, Wang AJ, Zhao JG. Multi-parametric MRI in cervical cancer: early prediction of response to concurrent chemoradiotherapy in combination with clinical prognostic factors. Eur Radiol. 2018;28(1):437–445. [PubMed: 28779395]

202. Gao S, Du S, Lu Z, Xin J, Gao S, Sun H. Multiparametric PET/MR (PET and MR-IVIM) for the evaluation of early treatment response and prediction of tumor recurrence in patients with locally advanced cervical cancer. Eur Radiol. 2020;30(2):1191–1201. [PubMed: 31493211]

203. Mahajan A, Engineer R, Chopra S, et al. Role of 3T multiparametric-MRI with BOLD hypoxia imaging for diagnosis and post therapy response evaluation of postoperative recurrent cervical cancers. Eu J Radiol Open. 2016;3:22–30.

204. Zhou H, Zhang Z, Denney R, et al. Tumor physiological changes during hypofractionated stereotactic body radiation therapy assessed using multi-parametric magnetic resonance imaging. Oncotarget. 2017;8(23):37464. [PubMed: 28415581]

205. Tao X, Wang L, Hui Z, et al. DCE-MRI perfusion and permeability parameters as predictors of tumor response to CCRT in patients with locally advanced NSCLC. Sci Rep. 2016;6(1):1–9. [PubMed: 28442746]

206. Huang Y-S, Chen J-Y, Hsu F-M, et al. Response assessment of stereotactic body radiation therapy using dynamic contrast-enhanced integrated MR-PET in non-small cell lung cancer patients. J Magn Reson Imaging. 2018;47(1):191–199. [PubMed: 28480541]

207. El Naqa I, Cuneo K, Owen D, Lawrence TS, Ten Haken RK. Radiation sensitivity of the liver: models and clinical data. Radiation therapy for liver tumors. Springer. 2017;39–47.

208. Wang H, Cao Y. Correction of arterial input function in dynamic contrast-enhanced MRI of the liver. J Magn Reson Imaging, 2012;36(2):411–421. [PubMed: 22392876]

209. Wang H, Farjam R, Feng M, et al. Arterial perfusion imaging–defined subvolume of intrahepatic cancer. Int J Radiat Oncol Biol Phys. 2014;89(1):167–174. [PubMed: 24613814]

210. El Naqa I, Johansson A, Owen D, et al. Modeling of normal tissue complications using imaging and biomarkers after radiation therapy for hepatocellular carcinoma. Int J Radiat Oncol Biol Phys. 2018;100(2):335–343. [PubMed: 29353652]

211. Kamel IR, Reyes DK, Liapi E, Bluemke DA, Geschwind J-FH. Functional MR imaging assessment of tumor response after 90Y microsphere treatment in patients with unresectable hepatocellular carcinoma. J Vasc Interv Radiol. 2007;18(1):49–56. [PubMed: 17296704]

212. Rhee TK, Naik NK, Deng J, et al. Tumor response after yttrium-90 radioembolization for hepatocellular carcinoma: comparison of diffusion-weighted functional MR imaging with anatomic MR imaging. J Vasc Interv Radiol. 2008;19(8):1180–1186. [PubMed: 18656011]

213. Weikert T, Maas OC, Haas T, et al. Early prediction of treatment response of neuroendocrine hepatic metastases after peptide receptor radionuclide therapy with 90Y-DOTATOC using diffusion weighted and dynamic contrast-enhanced MRI. Contr Media Molecul Imaging. 2019;2019.

214. Yeh R, Dercle L, Garg I, Wang ZJ, Hough DM, Goenka AH. The role of 18F-FDG PET/CT and PET/MRI in pancreatic ductal adenocarcinoma. Abdom Radiol. 2018;43(2):415–434.

215. Cuneo KC, Chenevert TL, Ben-Josef E, et al. A pilot study of diffusion-weighted MRI in patients undergoing neoadjuvant chemoradiation for pancreatic cancer. Translat Oncol. 2014;7(5):644–649.

216. Klaassen R, Gurney-Champion OJ, Engelbrecht MRW, et al. Evaluation of six diffusion-weighted MRI models for assessing effects of neoadjuvant chemoradiation in pancreatic cancer patients. Int J Radiat Oncol Biolo Phys. 2018;102(4)1052–1062.

217. Zimmermann C, Distler M, Jentsch C, et al. Evaluation of response using FDG-PET/CT and diffusion weighted MRI after radiochemotherapy of pancreatic cancer: a non-randomized, monocentric phase II clinical trial—PaCa-DD-041 (Eudra-CT 2009-011968-11). Strahlenther Onkol. 2020:1–8.

218. Liu Y, Wang Y, Tang W, Jiang M, Li K, Tao X. Multiparametric MR imaging detects therapy efficacy of radioactive seeds brachytherapy in pancreatic ductal adenocarcinoma xenografts. Radiol Med (Torino). 2018;123(7):481–488. [PubMed: 29508241]

219. Tomaszewski MR, Dominguez-Viqueira W, Ortiz A, et al. Heterogeneity analysis of MRI T2 maps for measurement of early tumor response to radiotherapy. NMR Biomed. 2021;34(3):e4454. [PubMed: 33325086]

220. Aoyagi T, Shuto K, Okazumi S, Shimada H, Kazama T, Matsubara H. Apparent diffusion coefficient values measured by diffusion-weighted imaging predict chemoradiotherapeutic effect for advanced esophageal cancer. Digest Surg. 2011;28(4):252–257.

221. Xie T, Ye Z, Pang P, Shao G. Quantitative multiparametric MRI may augment the response to radiotherapy in mid-treatment assessment of patients with esophageal carcinoma. Oncol Res Treat. 2019;42(6):326–333. [PubMed: 31064001]

222. Heethuis SE, Goense L, van Rossum PSN, et al. DW-MRI and DCE-MRI are of complementary value in predicting pathologic response to neoadjuvant chemoradiotherapy for esophageal cancer. Acta Oncol. 2018;57(9):1201–1208. [PubMed: 29781342]

223. Takagi H, Ota H, Umezawa R, et al. Left ventricular T1 mapping during chemotherapy–radiation therapy: serial assessment of participants with esophageal cancer. Radiology. 2018;289(2):347–354. [PubMed: 29989523]

224. Winfield JM, Miah AB, Strauss D, et al. Utility of multi-parametric quantitative magnetic resonance imaging for characterization and radiotherapy response assessment in soft-tissue sarcomas and correlation with histopathology. Frontiers in oncology. 2019;9:280. [PubMed: 31106141]

225. Spratt DE, Arevalo-Perez J, Leeman JE, et al. Early magnetic resonance imaging biomarkers to predict local control after high dose stereotactic body radiotherapy for patients with sarcoma spine metastases. Spine J. 2016;16(3):291–298. [PubMed: 26325017]

226. Sullivan DC, Obuchowski NA, Kessler LG, et al. Metrology standards for quantitative imaging biomarkers. Radiology. 2015;277(3):813–825. [PubMed: 26267831]

227. Winfield JM, Payne GS, Weller A, deSouza NM. DCE-MRI, DW-MRI, and MRS in cancer: challenges and advantages of implementing qualitative and quantitative multi-parametric imaging in the clinic. Top Magn Reson Imaging. 2016;25(5):245. [PubMed: 27748710]

228. Barnhart HX, Barboriak DP. Applications of the repeatability of quantitative imaging biomarkers: a review of statistical analysis of repeat data sets. Translational oncology. 2009;2(4):231–235. [PubMed: 19956383]

229. Shukla-Dave A, Obuchowski NA, Chenevert TL, et al. Quantitative imaging biomarkers alliance (QIBA) recommendations for improved precision of DWI and DCE-MRI derived biomarkers in multicenter oncology trials. J Magn Reson Imaging. 2019;49(7):e101–e121. [PubMed: 30451345]

230. Fowler JF. 21 years of biologically effective dose. Br J Radiol. 2010;83(991):554–568. [PubMed: 20603408]

231. Kirkpatrick JP, Meyer JJ, Marks LB. The linear-quadratic model is inappropriate to model high dose per fraction effects in radiosurgery. Semin Radiat Oncol. 2008;18(4):240–243. [PubMed: 18725110]

232. Hormuth DA, Jarrett AM, Lima EA, McKenna MT, Fuentes DT, Yankeelov TE. Mechanism-based modeling of tumor growth and treatment response constrained by multiparametric imaging data. JCO clinical cancer informatics. 2019;3:1–10.

233. Li X, Priest RA, Woodward WJ, et al. Feasibility of shutterspeed DCE-MRI for improved prostate cancer detection. Magn Reson Med. 2013;69(1):171–178. [PubMed: 22457233]

234. Wang C, Subashi E, Liang X, Yin F-F, Chang Z. Evaluation of the effect of transcytolemmal water exchange analysis for therapeutic response assessment using DCE-MRI: a comparison study. Phys Med Biol. 2016;61(13):4763. [PubMed: 27272391]

235. Bashat DB, Sira LB, Graif M, et al. Normal white matter development from infancy to adulthood: comparing diffusion tensor and high b value diffusion weighted MR images. J Magnet Reson Imaging Off J Int Soc Magn Reson Med. 2005;21(5):503–511.

236. Pineda F, Medved M, Fan X, et al. Comparison of dynamic contrast-enhanced MRI parameters of breast lesions at 1.5 and 3.0 T: a pilot study. Br J Radiol. 2015;88(1049):20150021. [PubMed: 25785918]

237. Zhan L, Mueller BA, Jahanshad N, et al. Magnetic resonance field strength effects on diffusion measures and brain connectivity networks. Brain connectivity. 2013;3(1):72–86. [PubMed: 23205551]

238. Xu G, Rowley HA, Wu G, et al. Reliability and precision of pseudo-continuous arterial spin labeling perfusion MRI on 3.0 T and comparison with 15O-water PET in elderly subjects at risk for Alzheimer's disease. NMR Biomed. 2010;23(3):286–293. [PubMed: 19953503]

239. Calamante F. Bolus dispersion issues related to the quantification of perfusion MRI data. J Magn Reson Imaging Off J Int Soc Magn Res Med. 2005;22(6):718–722.

240. Bane O, Hectors SJ, Wagner M, et al. Accuracy, repeatability, and interplatform reproducibility of T1 quantification methods used for DCE-MRI: Results from a multicenter phantom study. Magn Reson Med. 2018;79(5):2564–2575. [PubMed: 28913930]

241. Gurney-Champion OJ, Mahmood F, van Schie M, et al. Quantitative imaging for radiotherapy purposes. Radiother Oncol. 2020;146:66–75. [PubMed: 32114268]

242. Huang W, Chen Y, Fedorov A, et al. The impact of arterial input function determination variations on prostate dynamic contrast-enhanced magnetic resonance imaging pharmacokinetic modeling: a multicenter data analysis challenge. Tomography. 2016;2(1):56–66. [PubMed: 27200418]

243. Georgiou L, Wilson DJ, Sharma N, Perren TJ, Buckley DL. A functional form for a representative individual arterial input function measured from a population using high temporal resolution DCE MRI. Magn Reson Med. 2019;81(3):1955–1963. [PubMed: 30257053]

244. Benedict SH, Yenice KM, Followill D, et al. Stereotactic body radiation therapy: the report of AAPM Task Group 101. Med Phys. 2010;37(8):4078–4101. [PubMed: 20879569]

245. Jezzard P. Correction of geometric distortion in fMRI data. NeuroImage. 2012;62(2):648–651. [PubMed: 21945795]

246. Cao Y. The promise of dynamic contrast-enhanced imaging in radiation therapy. Semin Radiat Oncol. 2011;21(2):147–156. [PubMed: 21356482]

247. Yan D. Adaptive radiotherapy: merging principle into clinical practice. Semin Radiat Oncol. 2010;20(2):79–83. [PubMed: 20219545]

248. Leibfarth S, Winter RM, Lyng H, Zips D, Thorwarth D. Potentials and challenges of diffusion-weighted magnetic resonance imaging in radiotherapy. Clin Translat Radiat Oncol. 2018;13:29–37.

249. Troost EG, Thorwarth D, Oyen WJ. Imaging-based treatment adaptation in radiation oncology. J Nucl Med. 2015;56(12):1922–1929. [PubMed: 26429959]

250. Labeyrie M-A, Turc G, Hess A, et al. Diffusion lesion reversal after thrombolysis: a MR correlate of early neurological improvement. Stroae. 2012;43(11):2986–2991.

251. Bajpai J, Gamnagatti S, Kumar R, et al. Role of MRI in osteosarcoma for evaluation and prediction of chemotherapy response: correlation with histological necrosis. Pediatr Radiol. 2011;41(4):441–450. [PubMed: 20978754]
252. Wang C, Liu C, Chang Y, et al. Dose-distribution-driven PET image-based outcome prediction (DDD-PIOP): a deep learning study for oropharyngeal cancer IMRT application. Front Oncol. 2020;10:1592. [PubMed: 33014811]
253. Brock KK, Mutic S, McNutt TR. Li H, Kessler ML. Use of image registration and fusion algorithms and techniques in radiotherapy: report of the AAPM Radiation Therapy Committee Task Group No. 132. Med Phys. 2017;44(7):e43–e76. [PubMed: 28376237]
254. Mcjury M, O'Neill A, Lawson M, et al. Assessing the image quality of pelvic MR images acquired with a flat couch for radiotherapy treatment planning. Br J Radiol. 2011;84(1004):750–755. [PubMed: 21750138]
255. Raaymakers BW, Lagendijk JJW, Overweg J, et al. Integrating a 1.5 T MRI scanner with a 6 MV accelerator: proof of concept. Phys Med Biol. 2009;54(12):N229–N237. [PubMed: 19451689]
256. Cao M, Padgett KR, Rong Y. Are in-house diagnostic MR physicists necessary for clinical implementation of MRI guided radiotherapy? J Appl Clin Med Phys. 2017;18(5):6.
257. Barisano G, Sepehrband F, Ma S, et al. Clinical 7 T MRI: Are we there yet? A review about magnetic resonance imaging at ultra-high field. Br J Radiol. 2019;92(1094):20180492. [PubMed: 30359093]
258. Mirkes CC, Hoffmann J. Shajan G, Pohmann R, Scheffler K. High-resolution quantitative sodium imaging at 9.4 Tesla. Magn Reson Med. 2015;73(1):342–351. [PubMed: 24435910]
259. Ouwerkerk R, Bleich KB, Gillen JS, Pomper MG, Bottomley PA. Tissue sodium concentration in human brain tumors as measured with 23Na MR imaging. Radiology. 2003;227(2):529–537. [PubMed: 12663825]
260. Herk MV, McWilliam A, Dubec M, Faivre-Finn C, Choudhury A. Magnetic Resonance Imaging e Guided Radiation Therapy: A Short Strengths. Weaknesses, Opportunities, and Threats Analysis; 2018.
261. Oborn BM, Dowdell S, Metcalfe PE, Crozier S, Mohan R, Keall PJ. Future of medical physics: real-time MRI-guided proton therapy. Med Phys. 2017;44(8):e77–e90. [PubMed: 28547820]
262. Padilla-Cabal F, Georg D, Fuchs H. A pencil beam algorithm for magnetic resonance image-guided proton therapy. Med Phys. 2018;45(5):2195–2204. [PubMed: 29532490]

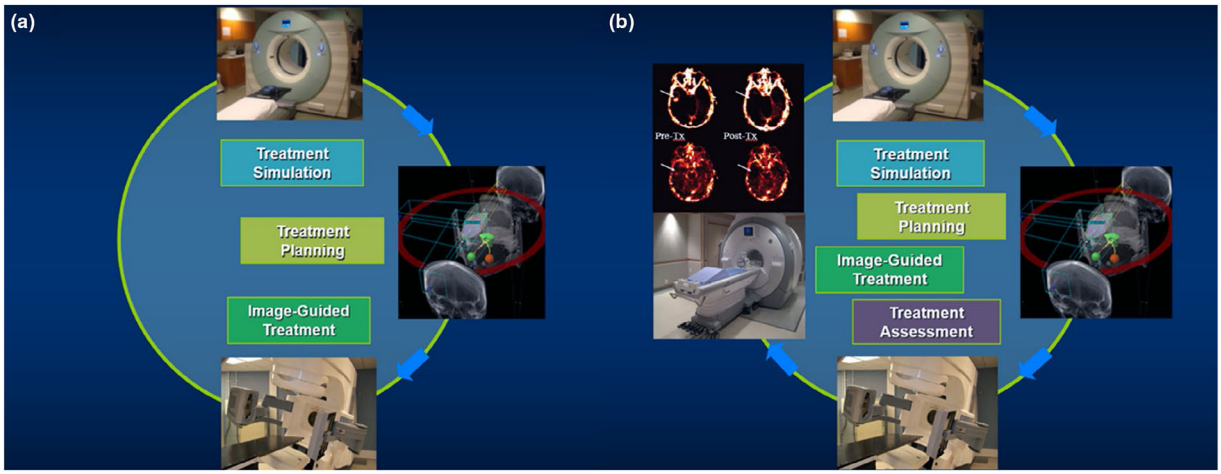

FIGURE 1.

(a) clinical workflow of radiation therapy (RT) in three stages: treatment simulation, treatment planning, and image-guided treatment; (b) proposed clinical flow of RT with an additional treatment assessment stage

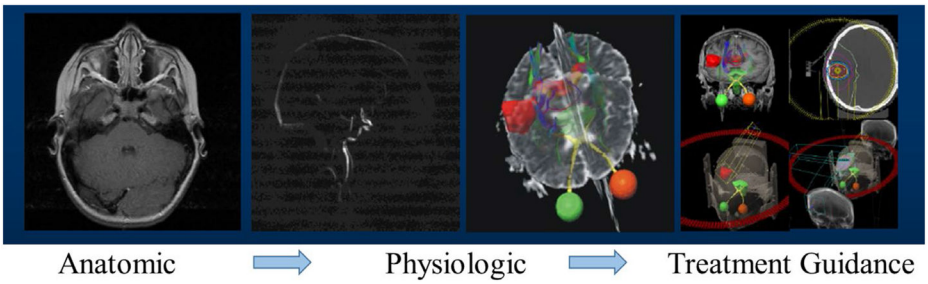

FIGURE 2.

An illustration of magnetic resonance imaging (MRI) evolution in brain arteriovenous malformation (AVM) stereotactic radiosurgery (SRS). In this application, anatomical MRI scans are acquired for general cranial anatomy evaluation. Two physiologic scans are adopted: two-dimensional/three-dimensional based MR angiography is acquired to identify target region(s), and diffusion tensor imaging (DTI) is acquired for tractography to identify nerve tracts avoidance candidates. On-board x-ray based imaging and potential MR imaging techniques can be used for accurate target positioning purpose during SRS administration

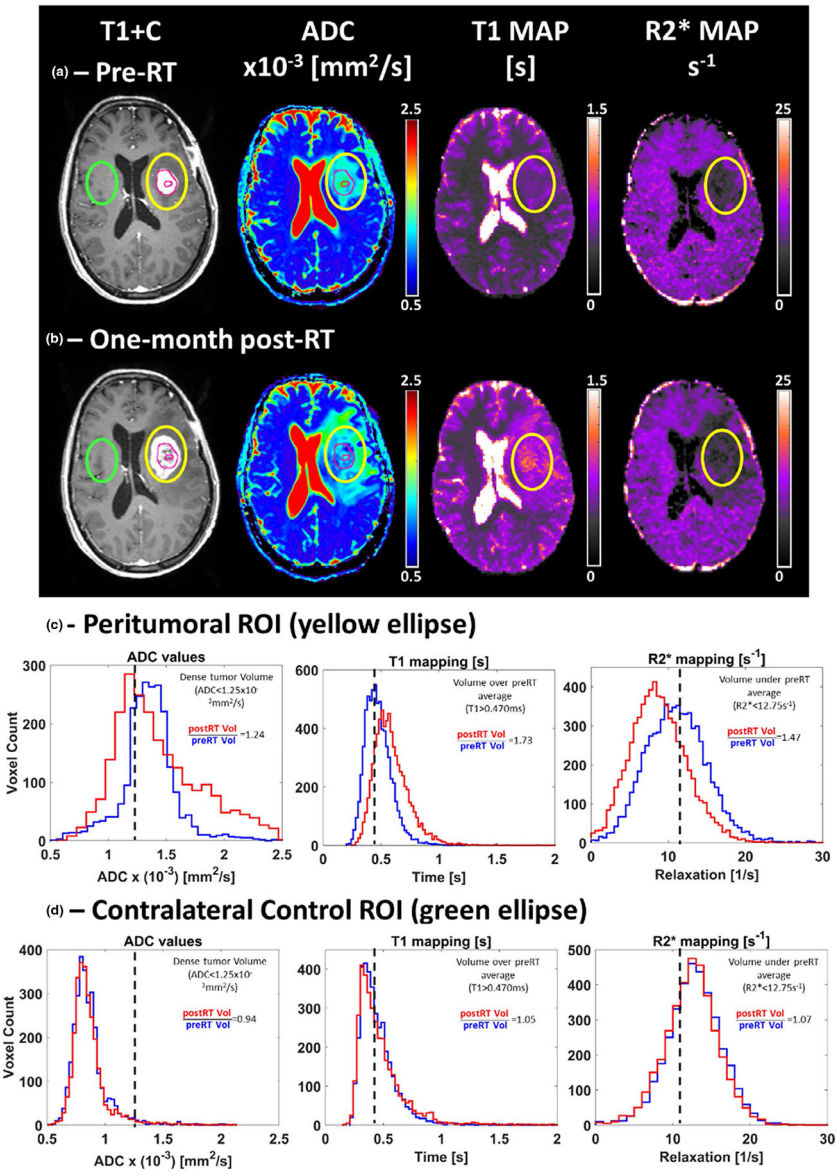

FIGURE 3.

An example of multiparametric magnetic resonance imaging (mpMRI) containing T1 post-contrast (T1+C), apparent diffusion coefficient (ADC), T1, and R2* maps estimated from data acquired pre (a) and one-month post-RT (b) from a 58-year-old woman with partially resected glioblastoma of the left temporal lobe. The DWI images used to estimate the ADC maps and the T1+C were acquired on a 3T Skyra (Siemens, Erlangen, Germany) clinical scanner and the data used to estimate T1 and R2* maps were obtained on a 0.35 T MRIdian (ViewRay, Cleveland, OH) combination MRI and RT system. The multiparametric analysis was performed for voxels within two different regions of interest (ROI). The yellow ellipse highlights the peritumoral ROI (c). The resection cavity and tumor original contrast-enhanced volume are highlighted by the inner and outer magenta circles within the peritumoral ROI, respectively. A contralateral control ROI (green ellipse) was also analyzed

by the multiparametric approach (d) in order to provide a measurement of each parameter's stability across different time points

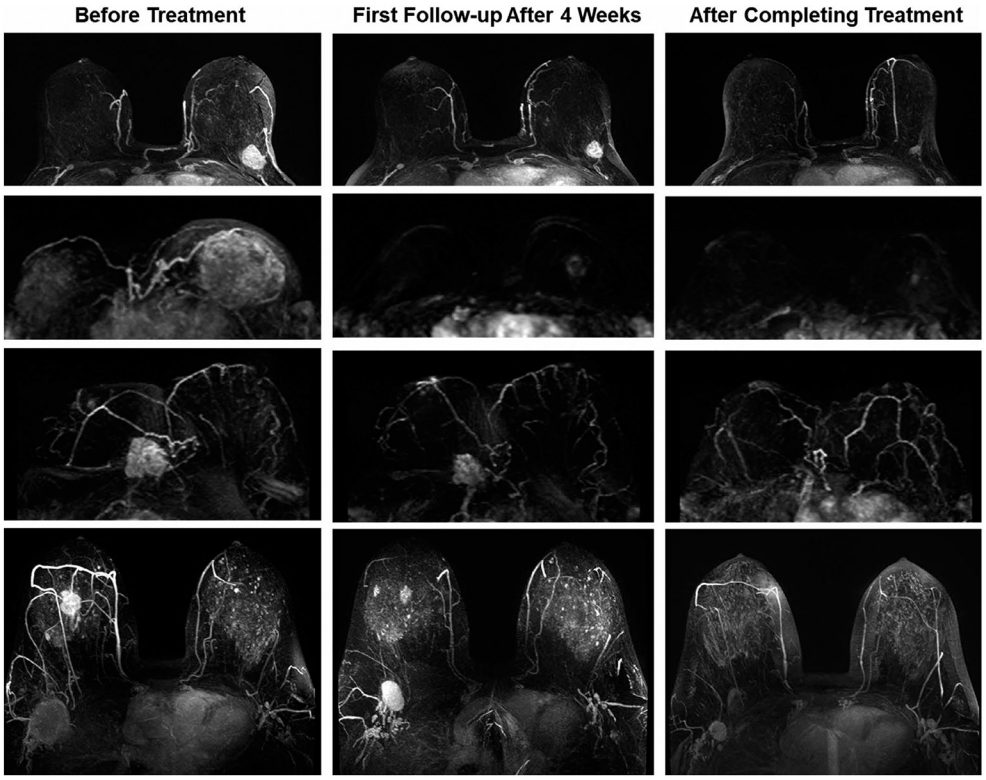

FIGURE 4.

Four case examples of breast cancer patients receiving neoadjuvant chemotherapy. The images are maximum intensity projection at baseline and follow-up examinations after 4 weeks and after completing the entire course. The top patient has an immediately operable tumor, but elects to receive NAC to facilitate surgery and achieve a better outcome. The second patient has inoperable cancer and shows a great response to NAC, which not only facilitates surgery but also further allows breast conservation. The third patient has an invasive lobular cancer, which appears to respond well; however, in the post-NAC specimen examination, the scattered cells are seen in the entire original tumor bed. For lobular cancer and non-mass lesions, minimum residual disease may present as scattered cells or cell clusters, and underestimated by magnetic resonance imaging. The last patient shows a complete response in primary cancer, but the partial response in the lymph node, suggesting the need for axillary dissection and axillary radiation

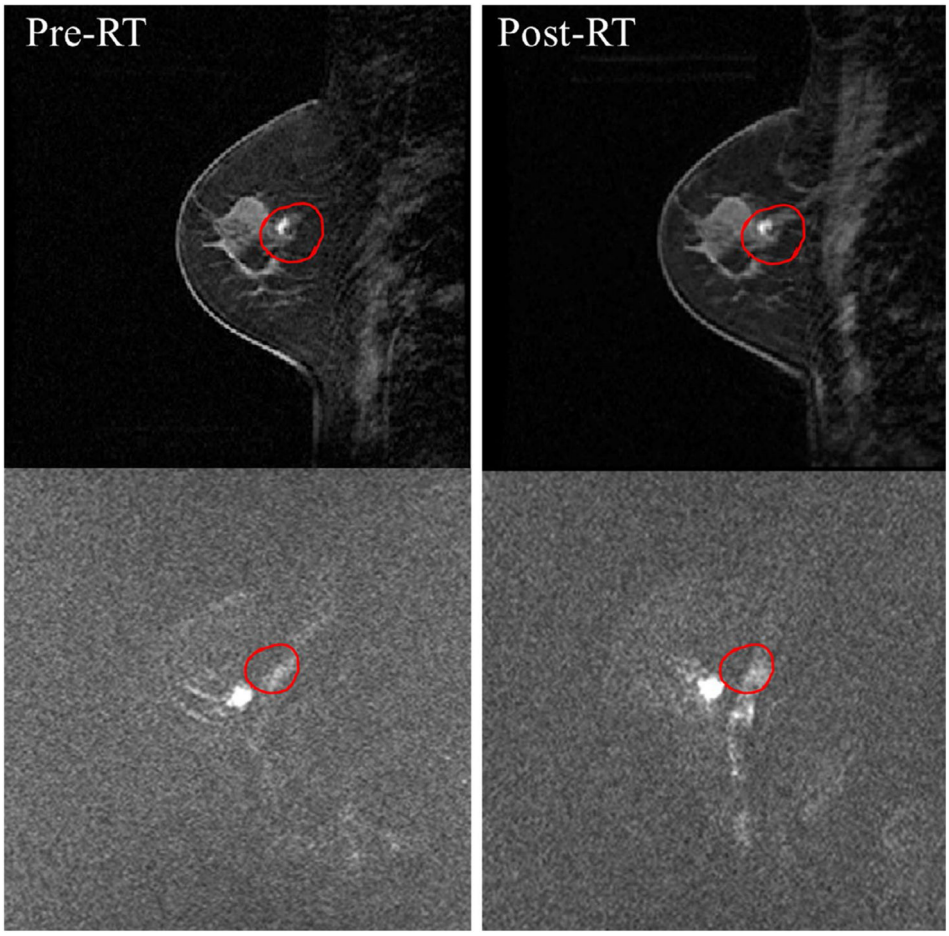

FIGURE 5.

A comparison of post-enhancement dynamic contrast enhanced (DCE)-magnetic resonance imaging (MRI) (top) and diffusion weighted imaging (DWI) (b = 500 mm2/s) (bottom) images before and after single-fraction delivery of stereotactic body radiation therapy. Red CTV contour is resampled in DCE-MRI and DWI coordinates, respectively

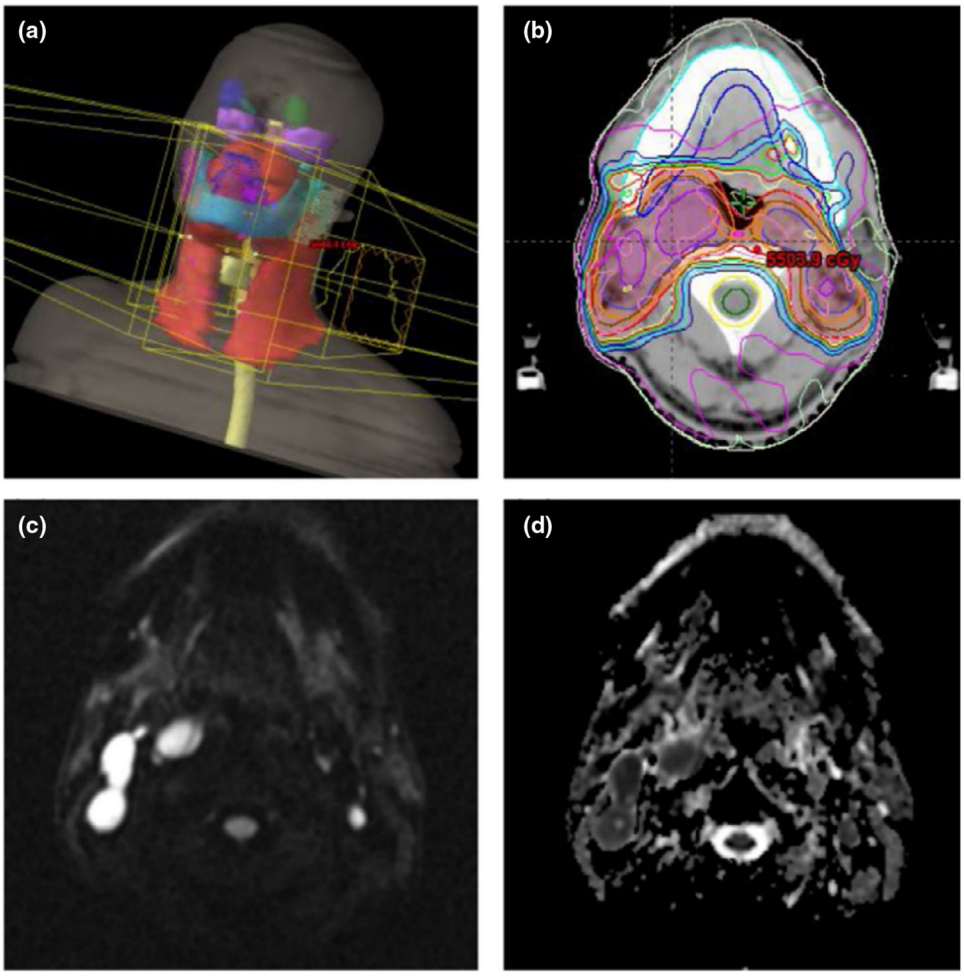

FIGURE 6.

An example HNC IMRT: (a) three-dimensional view of PTV in red; (b) PTV and dose distribution outlined on axial CT slice; (c) diffusion weighted imaging (DWI) image and (d) the corresponding ADC map assisted CTV delineation (purple segments) in (b)

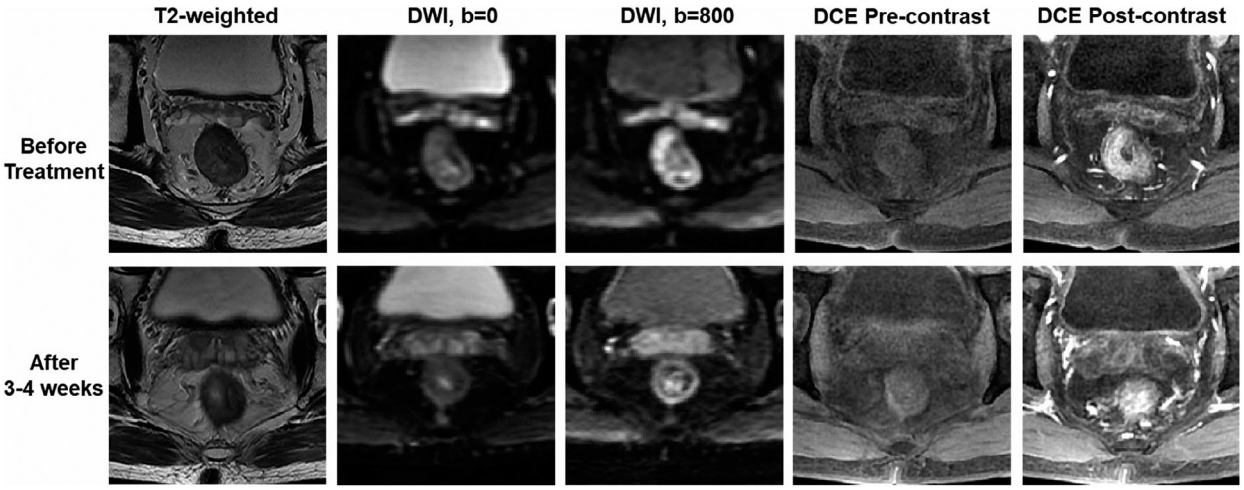

FIGURE 7.

multiparametric magnetic resonance imaging (mpMRI) acquired from a patient with locally advanced rectal cancer receiving neoadjuvant chemo-RT. After treatment, the signal intensity is decreased on diffusion weighted imaging (b = 800 mm2/s), suggesting the increase of apparent diffusion coefficient. The enhanced tumor area becomes smaller, also suggesting a good response